Bulletin of the Seismological Society of America, Vol. 101, No. 1, pp. 13–38, February 2011, doi: 10.1785/0120100050

San Andreas Fault Earthquake Chronology and Lake Cahuilla History at Coachella, California

by Belle Philibosian, Thomas Fumal, and Ray Weldon

Abstract The southernmost ~100 km of the San Andreas fault has not ruptured historically. It is imperative to determine its rupture history to better predict its future behavior. This paleoseismic investigation in Coachella, California, establishes a chronology of at least five and up to seven major earthquakes during the past ~1100 yr. This chronology yields a range of average recurrence intervals between 116 and 221 yr, depending on assumptions, with a best-estimate average recurrence interval of 180 yr. The most recent earthquake occurred c.1690, more than 300 yr ago, suggesting that this stretch of the fault has accumulated a large amount of tectonic stress and is likely to rupture in the near future, assuming the fault follows a stress renewal model. This study also establishes the timing of the past 5–6 highstands of ancient Lake Cahuilla since A.D. 800. We found that earthquakes do not tend to occur at any particular stage in the lake cycle.

Introduction

The Coachella Valley section of the San Andreas fault (SAF), between San Gorgonio Pass and the Imperial Valley, is the only noncreeping portion of the 1300-km-long fault that has not ruptured in a major earthquake during historical time (Fig. 1). For this reason, the hazard potential and likely timing of its next earthquake are poorly constrained in comparison to other sections of the fault, since these parameters must be determined solely from paleoseismology. Paleoseismic analysis of the southernmost SAF is particularly important because a rupture on this fault segment has the potential to severely damage the adjacent Los Angeles metropolitan area, particularly if the rupture propagates northward through the San Gorgonio Pass (Olsen *et al.*, 2006). In addition, rupture history is key to resolving important issues in fault behavior such as periodicity, segmentation, and characteristic versus random rupture behavior (discussed in Weldon *et al.*, 2004). Toward these ends, we have constructed an earthquake chronology for the past ~1200 yr for the southernmost SAF based on a new paleoseismic investigation conducted in the city of Coachella, California.

To date, there have been three other paleoseismic investigations on the SAF south of the San Gorgonio Pass (Fig. 1c), two of which have yet to be completely published. Sieh (1986) reported four earthquakes since A.D. 1000 from an investigation in the city of Indio, only a few kilometers northwest of the Coachella site. An ongoing investigation at Salt Creek, 45 km to the southeast of the Coachella site, includes evidence for six earthquakes since A.D. 800 (Williams, 2009), but specific dates for these have not yet been published. To date, the best record of Coachella Valley earthquakes comes from an extensive investigation 20 km to the northwest of the Coachella site at the Thousand Palms oasis, where Fumal, Rymer, and Seitz (2002) described evidence for five earthquakes since A.D. 800. However, in that region there are at least two active strands of the fault (Banning and Mission Creek), and only the Mission Creek strand passes through the Thousand Palms site. The Mission Creek strand gradually dies out to the northwest, with slip becoming concentrated on the Banning strand. While the Mission Creek strand has a slip rate between 12 and 22 mm/yr at the Biskra Palms site, which is located in the junction zone between the two strands (Behr *et al.*, 2010), its slip rate at the Thousand Palms site is only a few millimeters per year (Fumal, Rymer, and Seitz, 2002), with the Banning strand likely accommodating the majority of the slip. The two strands probably move in concert, but it is possible that the Thousand Palms site record is missing earthquakes that produced surface rupture only on the Banning strand. The Coachella site, located to the southeast in the region where the SAF is singly stranded, does not suffer from this source of ambiguity.

The most recent earthquake recorded at the Indio site has been dated to approximately A.D. 1680 (Sieh, 1986), more than 300 yr ago. This is significantly longer than most estimates of average recurrence interval of on other segments of the fault, which range from ~100 to 250 yr (e.g., Sieh *et al.*, 1989; Weldon *et al.*, 2004; Weldon *et al.*, 2005; Kelson *et al.*, 2006; Goldfinger *et al.*, 2008; Akciz *et al.*, 2009). This open interval is about as long as the longest interval between earthquakes estimated by Sieh (1986) at the Indio site, and longer than any of the estimated interseismic intervals at the Thousand Palms site (Fumal, Rymer, and Seitz, 2002).

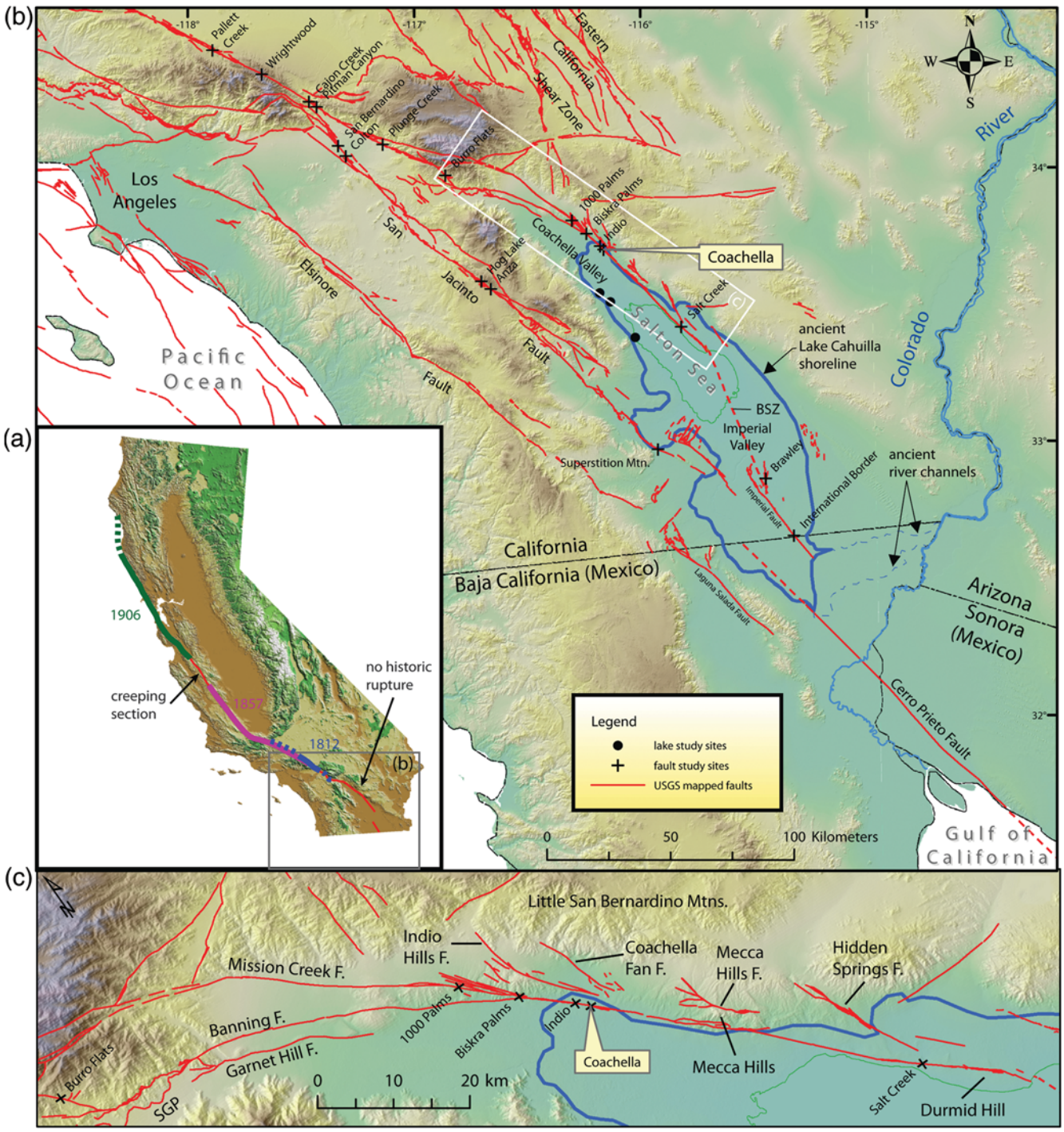

Figure 1. (a) Shaded relief map of California showing large historic ruptures of the San Andreas Fault. (b) Shaded relief map of southern California showing known Quaternary faults (from U.S. Geological Survey and California Geological Survey, 2006), major fault study sites, ancient Lake Cahuilla shoreline (heavy blue line), lake study sites (from Waters, 1983), and ancient alternate channels of the Colorado River which periodically filled the lake in the past. Only faults that are extensions of the San Andreas fault system are shown in Mexico. BSZ: Brawley seismic zone. (c) Shaded relief map showing the Coachella Valley section of the SAF, and associated nearby faults. SGP: San Gorgonio Pass.

This long period of quiescence has led many to suspect that an unusually large amount of elastic strain has built up along the southern San Andreas segment, and thus it is likely to produce a large to great (M_w 7–8) earthquake in the near future (Working Group on California Earthquake Probabilities, 2008).

The Coachella Paleoseismic Site

The Coachella site lies just southwest of the junction of Dillon Road and Avenue 44 in the city of Coachella. It is one of the few as yet undeveloped pieces of land on a stretch of the fault that is attractive for paleoseismology because slip

is concentrated on a single strand, whereas the structure diverges into several strands and becomes increasingly complex to the northwest toward San Gorgonio Pass (U.S. Geological Survey and California Geological Survey, 2006). The site lies at ~9 m elevation, just below the 12-m-high shoreline of the ancient Lake Cahuilla, which has intermittently filled by natural diversion of the Colorado River over the past several thousand years (e.g., Van de Kamp, 1973; Waters, 1983). While this site is one of the best-preserved stretches of the fault in the vicinity, there have been many anthropogenic alterations to the natural landscape. Now largely obliterated in this area, the ancient highstand shoreline can easily be identified ~0.5 km north of the site on stereo aerial photographs of the region taken in 1939 (Fig. 2a), marked by an elevated beach berm and vegetated dunes. The Indio Canyon wash (which drains alluvial fans exiting the Little San Bernardino Mountaing to the north) passes through the site and is prominent in this photograph. However, when the Coachella Canal was constructed in the 1940s the wash outflow was permanently routed through flood control structures into Wasteway Number 3 to the west (Fig. 2b). The trace of the SAF is also easily identifiable in both the 1939 and 1951 photos as a sharp color and/or vegetation contrast. Because of extensive agriculture and other development, the surface trace is no longer easily identifiable in most of the area covered by these photographs (Fig. 2c). Also, the diversion of ground and surface water by flood control structures has led to a loss of vegetation, which has made the surface trace less prominent even in places where it has not been directly disturbed. However, small scarps up to 50 cm in height along with a marked contrast in vegetation density were still preserved at the minimally disturbed Coachella site. High-resolution topographic data from the B4 LiDAR (Light Detection and Ranging) dataset, collected in 2004 (Bevis *et al.*, 2006), show these and other features in detail (Fig. 3).

During an extensive Alquist-Priolo investigation on this property in March–April 2006, we were granted permission to use the trenches for a more detailed paleoseismic analysis. Though our analysis of this site was limited by time constraints and by lack of control over the excavation locations and procedures, this was a rare opportunity to work in very long, deep trenches excavated across the SAF trace within lacustrine and alluvial deposits. Three trenches trending N40°E, approximately perpendicular to the fault, were excavated across the entire property (locations shown in Fig. 3). The trenches were 7–8 meters deep and benched at ~1.5 m depth intervals, making the riser walls ~10 m apart at the top and ~2 m apart at the bottom (Fig. 4). The western most trench did not cross the main fault, with only minor faulting apparent at its northeastern end and essentially no deformation over the 400-m length of trench to the southwest. The easternmost trench revealed two fairly simple fault zones ~75 m apart, with no other deformation or offset visible along the 200-m length of the trench. Because datable material was rare and extensive erosion between lacustrine

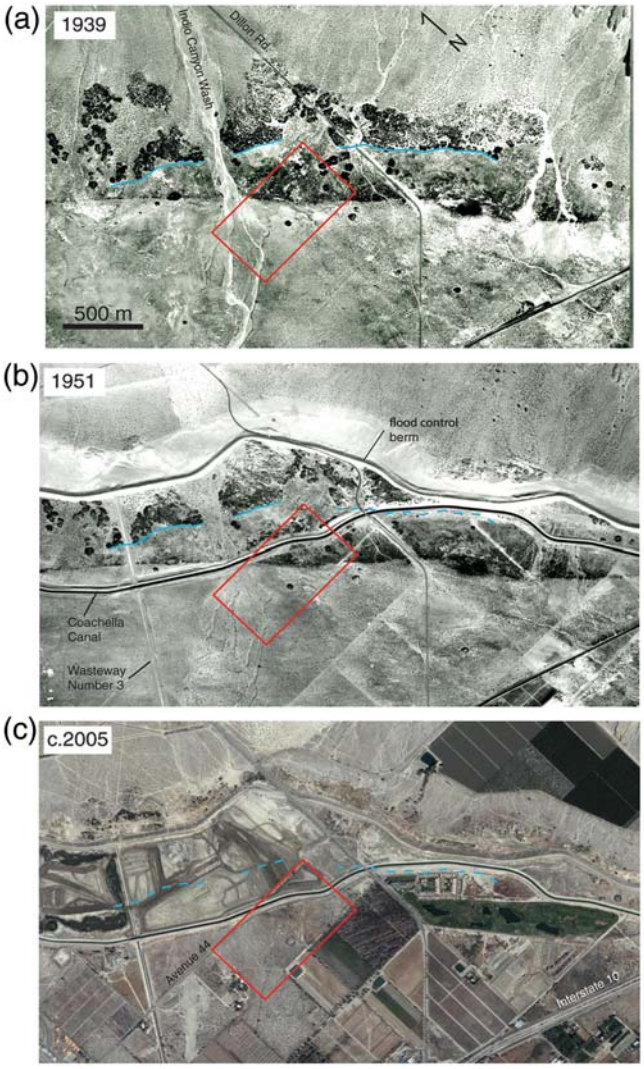

Figure 2. Historical aerial views of the study area. Ancient Lake Cahuilla highstand shoreline is outlined in blue and the Coachella site (area shown in Fig. 3) in red. The SAF trace is visible as a striking vegetation lineament in the two earlier photographs, but is preserved only at the Coachella site in the modern photograph. (a),(b) Photos courtesy of Sladden Engineering; (c) photo from Google Earth.

intervals makes the stratigraphic section incomplete, this trench was less than ideal for paleoseismic analysis. We photographed the walls of the eastern trench but did not analyze them in detail. The focus of our work was a detailed analysis of the three fault zones exposed in the central trench, where a largely complete stratigraphic section is preserved within a fault-bounded depression containing plentiful datable material. We found no significant deformation along the trench walls that extended for 250 m to the southwest of the logged section, only widely spaced fractures with little to no apparent vertical displacement. Exposure to the northeast of the 70-m logged section was limited by Avenue 44 and the Coachella Canal, so it is possible that there are additional minor fault strands in that direction, but none are obvious on the 1939 aerial photo (Fig. 2a). Overall, we are confident

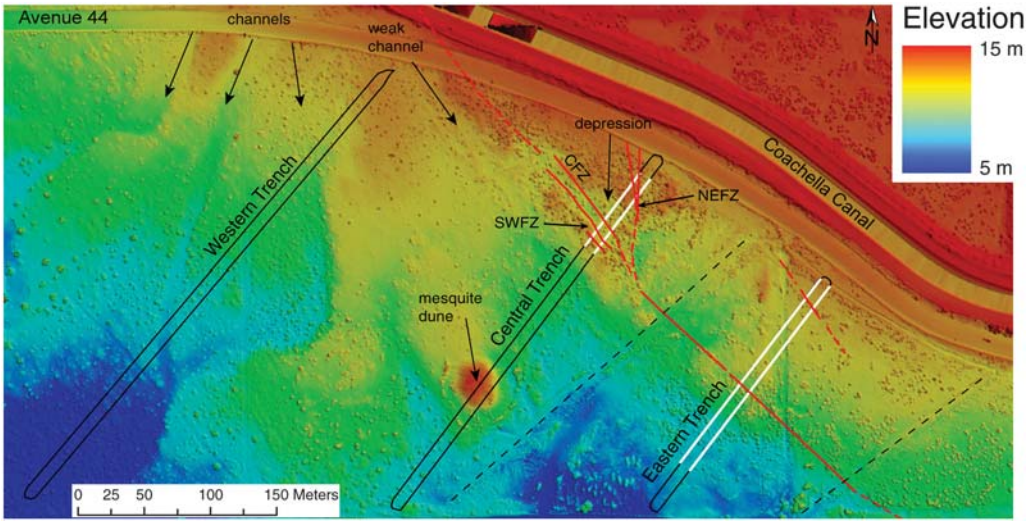

Figure 3. LiDAR topography (from the B4 project) of the study site. Trenches excavated for the 2006 Alquist–Priolo study are outlined in black. We photo-documented the trench walls marked in white. Walls in the central trench were analyzed in detail; in the eastern trench only the areas in the immediate vicinity of the two fault zones were analyzed in detail. Faults are mapped based on geomorphology/vegetation and trench exposures, including locations based on two earlier trenches excavated by Sladden Engineering in 2004 (Sladden Engineering, personal commun., 2006). The spoils from these earlier trenches can be seen in the LiDAR topography and are marked by dashed black lines. The now-blocked-off channels of Indio Canyon wash are visible at the left, as well as a weak channel along the fault scarp that was most likely the source of the thick channel deposit (unit 7S southwest) present at the southwest end of the logged portion of the central trench. The structural depression between the fault traces can be seen as a topographic low near the northeast end of the central trench. SWFZ: southwest fault zone, CFZ: central fault zone, NEFZ: northeast fault zone.

that our study encompasses all the major strands of the fault at this location.

We laid a 1 by 0.5 m string grid over a 70-m-long section of the central trench, covering each of the 5 bench risers on each wall. Each grid rectangle was individually photographed, and the ~1600 photographs were assembled into mosaics for each wall (Philibosian *et al.*, 2009). This area is unusually rich in datable materials, including organic soil and/or burn horizons (which theoretically provide *in situ* carbon-14 dates), plentiful detrital charcoal, and several types of freshwater shells from Lake Cahuilla.

Figure 4. View looking southwest along the central trench. Note that the fault is a highly effective groundwater barrier: the water table is about 6 m below the surface northeast of the central fault zone, which crosses the trench where the people are standing, but the trench is dry to the southwest. The benched excavation revealed a total vertical exposure of ~7 m.

Stratigraphy

The strata visible in the trench wall exposures alternate between fine-grained, often laminar deposits of Lake Cahuilla and subaerial fluvial and aeolian deposits that accumulated during periods when the lake receded below the elevation of the site. The exposed sediments are unlithified and composed largely of quartz and feldspar grains; fine-grained sediments are almost universally highly micaceous. Because this site is just a few meters below the highstand shoreline of the lake, lacustrine deposits represent periods of time when the lake basin was almost completely full (limited by the 12-meter-elevation sill separating the Salton Trough from regions draining to the Gulf of California). Thus, subaerial intervals do not necessarily imply that the entire lake basin desiccated, only that the influx from the Colorado River ceased for a time. The exposures revealed deposits from at least five lake highstands with intervening subaerial deposits. Figure 5 shows a generalized stratigraphic section for the Coachella site with descriptions of each unit. Each lacustrine unit is interpreted to be the product of a single lake highstand, while subunits represent variations in sediment delivery or other secondary environmental factors. The lacustrine-subaerial cycles are numbered in order of increasing stratigraphic depth with the letters S and L indicating subaerial and lacustrine layers, respectively.

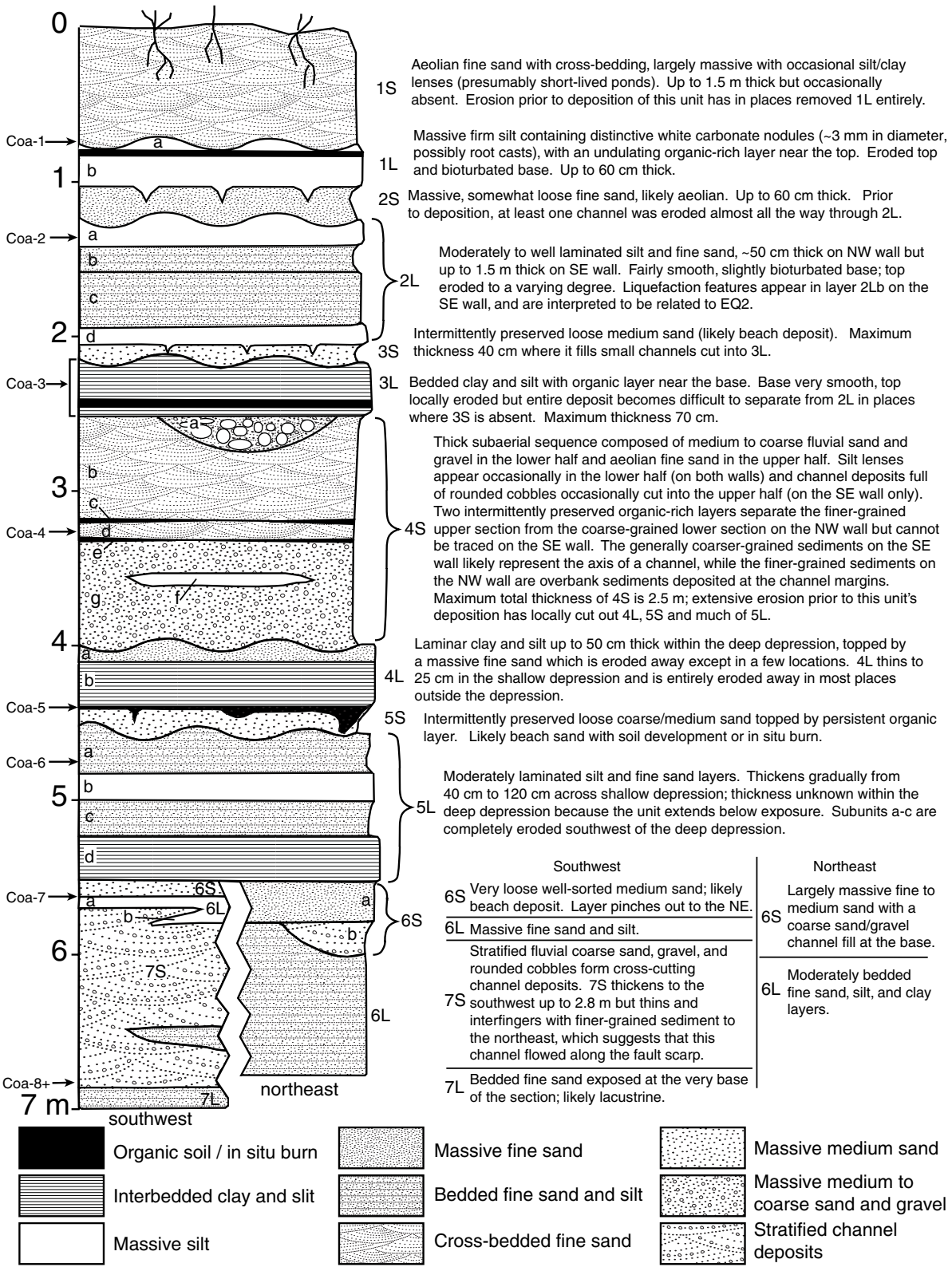

Figure 5. Generalized stratigraphic section of central trench exposures. Unit thickness is averaged over all logged exposures, excluding highly eroded areas. L and S indicate lacustrine and subaerial sediment, respectively. Wavy lines represent erosional contacts. Units below 5L are exposed only at the northeast and southwest ends of the logged exposures outside the structural depression, making correlation questionable, so separate stratigraphic sections are shown for each end. Numbered earthquake horizons (prefaced with Coa-) are indicated on the left side of the column.

Thicknesses of units shown in this section represent the average over the logged exposures (excluding areas where units were clearly substantially eroded). Variations from the average are large and the full range of unit thickness is noted in the description. Both the lacustrine and subaerial deposits commonly thicken across the depression-bounding faults, becoming 2 to 3 times thicker within the depression. This depression provides the most complete section without obvious hiatuses in deposition or major removal of section by erosion. In contrast, outside the depression, several of the lacustrine units are thinned or entirely removed by erosion. The high-resolution stratigraphy preserved within the depression includes many subunits that cannot be discerned outside the depression. These depression-filling deposits preserve the best expression of individual earthquake horizons.

Lacustrine deposits are identified by cohesive, often thinly bedded layers of well-sorted fine sand, silt, and clay. Ripple marks are present near the bases of some lacustrine units, likely reflecting lake transgression. It is generally believed that all lakes during this period initially rose to the same 12-meter level, controlled by the stable height of the sill formed by the Colorado River delta (e.g., Waters, 1983). Therefore, when the lake was at highstand, the depositional surface at this site would have been at a minimum of 3 meters depth, and even deeper for older units when less sediment had accumulated, meaning that the lacustrine deposition would not have been interrupted by very small fluctuations in lake level or shoreline processes such as wave action. The lower contacts of lacustrine units are generally smooth, though locally bioturbated (most likely by Lake Cahuilla mollusks). Internal erosional contacts never occur within a single lake unit. These fine-grained, well-bedded lacustrine sediments were additionally identifiable based on their tendency to retain moisture, causing them to appear considerably darker than the dry subaerial units and to precipitate a crust of salt crystals in a matter of hours as the exposed trench walls dried.

Subaerial deposits at this site include both aeolian and fluvial sediments. Aeolian deposits are characterized by loose, massive, locally cross-bedded, well-sorted fine sand and silt, while fluvial deposits consist of loose, thickly bedded, moderately to poorly sorted medium to coarse sand, pebbles, and rounded cobbles. The lower contacts of subaerial units are generally erosional contacts, often including channels carved into the underlying lacustrine units. Internal erosional contacts are common in the subaerial units, in contrast to the lacustrine units. Rip-up clasts and local mud cracks further support the identification of these deposits as subaerial. The fluvial deposits likely came from Indio Canyon wash. Sediment lobes and fluvial channels associated with this drainage remain visible in the topography (see Fig. 3). Influx from the wash likely produced a high local rate of sedimentation at this site (averaging ~5 mm/yr based on the dates obtained and presented in the following text). A few layers composed of very loose, massive, well-sorted medium sand are likely beach deposits (3S, 5S, and 6S southwest on Fig. 5). This interpretation is supported by their location as relatively thin intervals between lacustrine deposits.

Layer thickness and facies vary tremendously even over distances of a few meters, making lateral correlation of some units challenging. (Unfortunately, no fault-parallel trenches were available for this study). The uppermost units (1S and 1L) are sufficiently undeformed and intact so that we may confidently correlate them across the trench. We are also fairly confident in our cross-trench correlations of the lower units (numbered 4 and 5), because the trench walls were only ~2 m apart at the base. However, the intermediate units (numbered 2 and 3) are at levels where the trench was 7–8 m wide and are displaced substantially across faults, so cross-trench correlations (especially of individual subunits within a lake deposit) are not completely certain. In some cases, subunits that appear on one wall are entirely absent on the opposite wall, or change substantially in character over the intervening distance to be unrecognizable. Units below 5L are exposed only at the northeast and southwest ends of the logged exposures, outside the depositional depression. Substantial differences in the character of these deposits make correlation questionable across the depression so separate sections are shown for the southwest and northeast areas. The age of these deposits (discussed in the following text) coupled with slip rate estimates of at least 1 cm/yr (van der Woerd *et al.*, 2006; Behr *et al.*, 2010) implies that they have been laterally offset across the fault by tens of meters, juxtaposing sediments that potentially correlate in time but were formed in substantially different local environments. Unfortunately, the northeast section was almost entirely devoid of datable material, so correlation between the two basal sections by means of age control is not possible.

Fault Structure

Figure 6 presents summary logs of both walls of the central trench showing the geometry of the sedimentary deposits and fault zone structure. The three fault zones exposed in the central trench form a structural depression with reverse separation at its margins. The central and southwestern fault zones, striking approximately N40°W, bound the deepest ~10-m-wide portion of the depression, in which units are as much as three times thicker than corresponding units outside the depression to the southwest. While all faults are dominantly strike-slip, the down-dropping of the block between the faults clearly created considerable accommodation space for additional sediment, suggesting a transtensional pull-apart basin. The slight right-step of the fault trace visible in the 1939 aerial photo (Fig. 2a) also suggests a transtensional environment. However, both bounding faults dip 50°–60° away from the depression and thus have minor reverse vertical separation rather than the expected normal vertical separation. These faults are inferred to reverse their

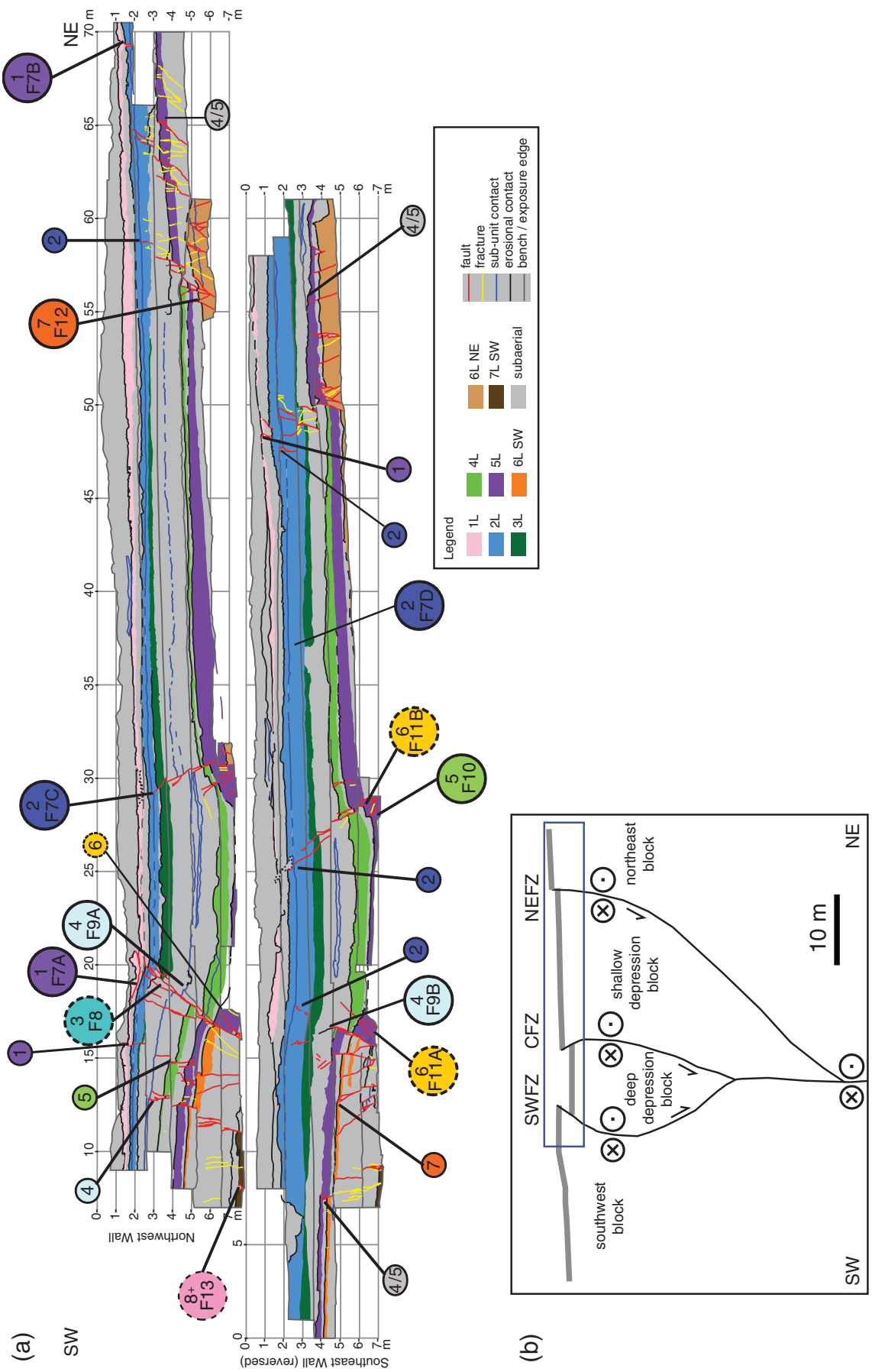

Figure 6. (a) Summary logs of the central trench showing the geometry of the sedimentary deposits and fault zone structure. View looking northwest; southeast wall has been reversed. Numbered circles show locations of earthquake evidence and Figures 7–13. (b) Schematic representation (looking northwest) of the inferred subsurface tulip structure. Box outlined in blue shows area exposed in the trench wall. The southwest, central, and northeast fault zones exposed in the central trench are abbreviated SWFZ, CFZ, and NEFZ, respectively. The overall downward surface slope from northeast to southwest is the regional gradient and is not related to local fault structure.

dip direction at depth to form a tulip structure (Naylor *et al.*, 1986; Sylvester, 1988) as shown in Figure 6b.

Northeast of the central fault zone, the depression shallows gradually for about 30 m (represented by the gradual thinning of deposits) until it is truncated against the complex northeastern fault zone, which strikes approximately northward, far from perpendicular to the trench walls (see Fig. 3). This fault zone dips very steeply to the west. The consistent east-side-up separations suggest that this strand has a normal component. Sediments are thinner and more substantially eroded in the hanging wall of this fault zone outside the depression. The strike of this fault zone suggests that it may connect to another strand of the SAF farther northeast (which, if it exists, would now be covered by Avenue 44 or the Coachella Canal), or even may be related to slip transfer off the main SAF to the Indio Hills fault, a nearby subparallel structure that bounds the Indio Hills on the northeast (see Fig. 1c). Unfortunately, the trace of this northward-striking strand is not clearly visible on the aerial photographs.

There is a notable difference between the southwest fault zone on the northwest and southeast walls. On the northwest wall, the southwest fault zone (SWFZ) appears to be the most active of the three, with two major strands breaking the three most recent lake deposits and larger apparent separation of units. However, on the southeast wall the youngest layer faulted by the SWFZ is 4S, with only minor fractures breaking the 2L and 3L lake deposits and none at all breaking the youngest lake deposit, though 2L and 3L do appear to be monoclinally folded. This suggests that this strand may be dying out to the southeast, which is somewhat surprising given that the southwestern strand would be expected to dominate southeast of a transtensional stepover. In contrast, the central and northeast fault zones appear relatively similar from wall to wall.

Earthquake Evidence

Evidence for past earthquakes at the Coachella site includes upward terminations of major fault strands that vertically separate lower units, sediment-draped scarps, filled fissures, liquefaction-related sedimentary structures, unit thickness and facies changes across faults, growth strata, and downward increase of vertical separation of units. We identify layers or contacts between layers that preserve multiple event indicators as probable earthquake horizons (i.e., were at the ground surface when an earthquake occurred). While subaerial ground ruptures generally disrupt the surface sufficiently so that the earthquake horizon is clear, sublacustrine earthquake horizons can be more subtle (e.g., Pezzopane and Weldon, 1993; Langridge *et al.*, 2000). At the Coachella site, it is sometimes the case that a fault offsets the bottom but not the top of a massive layer, either because sedimentation was continuous before and after the earthquake, or because the surface manifestation of faulting was obliterated by water action or plastic deformation. In such cases, the earthquake horizon cannot be determined more precisely than being within a certain layer. Even in cases where precise contacts between faulted and unfaulted strata can be identified, these contacts are usually not traceable over long lateral distances and thus may not correspond to the contacts used to delineate the major stratigraphic units. Therefore, most earthquakes are identified as having occurred during the deposition of a particular unit or subunit, rather than at a contact.

Because this segment of the fault is known to creep aseismically (Sieh and Williams, 1990; Lyons and Sandwell, 2003) at a rate of several millimeters per year, it is likely that in the centuries following an earthquake, some fractures continue to propagate upward into sediments deposited after the earthquake. This phenomenon could potentially lead to misidentification of paleocreep as a paleoearthquake. However, only one fault strand at the Coachella site continues all the way to the surface through the modern dune deposits (see Fig. 7a), most likely a result of the ~1 m of creep (estimated at the nearby Indio site) since the most recent earthquake (Sieh and Williams, 1990). This and other observations (Rymer *et al.*, 2002 and references therein) suggest that aseismic creep in this region usually occurs on a single fault strand or very narrow zone, so multiple fault strands that terminate at the same sedimentary layer are strong evidence for a seismic event even on a fault that occasionally creeps at the surface. We do not consider a single upward termination of a fault to be sufficient evidence of an earthquake horizon, because fault splays do not always rupture to the surface even in seismic events (McCalpin *et al.*, 2009 and references therein). Minor fractures that decrease downward and frequently do not reach the bottom of the trench are not considered meaningful event evidence either, because they likely form due to very local stresses and do not connect to the main fault. For these reasons, we require multiple pieces of spatially separated evidence in order to identify a particular layer as an earthquake horizon. We count fault terminations separately on each wall, because the walls are sufficiently far apart to allow strands to merge or diverge in the intervening space.

Central Trench Earthquake Evidence

There is excellent evidence exposed on the walls of the central trench for five earthquakes and some evidence for three additional earthquakes (see Fig. 6a). These potential earthquake horizons are given the prefix Coa- for Coachella and are numbered in order of increasing stratigraphic depth. There is a variety of evidence types for Coa-1, -2, -4, -5, and -7 at multiple locations, so we infer these five events to be probable earthquakes. Evidence for Coa-3, -6, and -8+ is less direct and more limited in spatial distribution, so these are evaluated as possible earthquakes. Earthquake evidence is described in the following text and summarized in Table 1. We employ a system similar to that used by Scharer *et al.* (2007) to rank each piece of evidence from 1 to 4 based on quality. High-quality evidence can only be explained

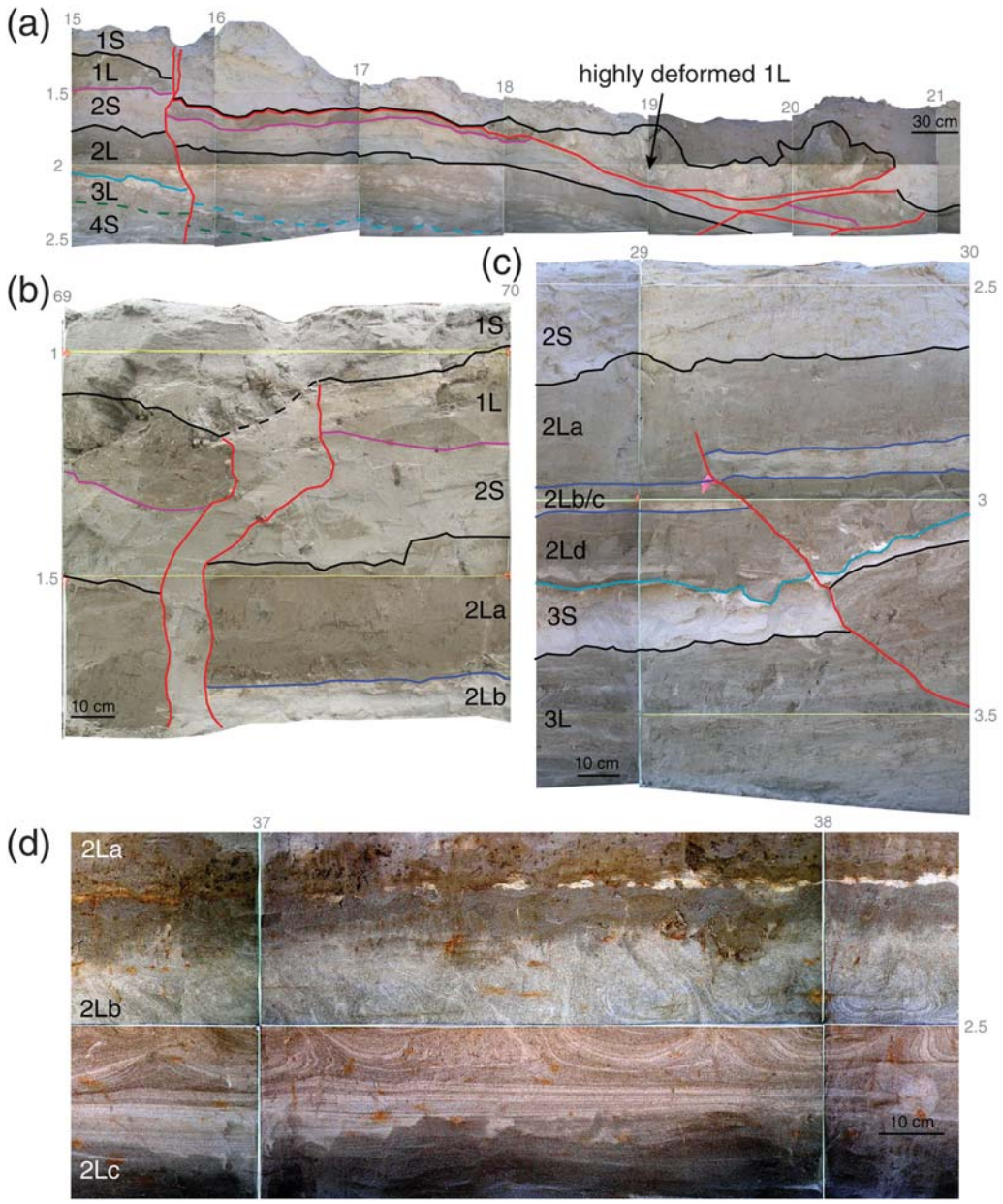

Figure 7. (a–b) Evidence for the most recent earthquake, Coa-1. (a) Northwest wall, riser 1, meters 15–21 showing the slump deposit in unit 1L. The vertical fault at the left also may have broken during Coa-1, but the fractures that extend into unit 1S must be due to more recent aseismic creep. (b) Northwest wall, riser 1, meters 69–70 showing a fissure breaking units 1L and 2L filled with subaerial material. (c–d) Evidence for Coa-2. (c) Northwest wall, riser 2, meters 29–30 showing substantial offset of 3L, 3S, and lower lake 2 subunits and the undeformed top of unit 2L. (d) Southeast wall, riser 2, meters 37–38 (reversed) showing liquefaction features in unit 2Lb.

by an earthquake, and unambiguously delineates the earthquake horizon. Upward terminations are rated 1 or 2 depending on the magnitude of the separation near the tip, because those with large separations that end abruptly are more indicative of a surface rupture (marking a true earthquake horizon) than those which express tapering separation. Liquefaction features and abrupt thickness change of units are generally ranked 3, because they are strong evidence for an earthquake but do not mark the earthquake horizon precisely. Features such as sediment slumps, fissures, and fault terminations associated with clear deformation contrasts are ranked 4, because they must be associated with earthquakes and mark earthquake horizons definitively. To be accepted as a probable earthquake, there must be at least one piece of evidence ranked 4, or the total rank must be greater than 8. The best pieces of evidence are shown in Figures 7–13; others are marked on Figure 6a and can be found on the complete trench logs in Philibosian *et al.* (2009). It is also important to note that earthquake evidence which could be due to more than one of the listed earthquakes is not included in the table and descriptions (e.g., faults that terminate at local unconformities where significant

Table 1
Ranked Evidence for Paleoearthquakes

Earthquake	Description	Rank	Wall	Riser	Meters	Figure
Coa-1	Soft-sediment detachment slump	4	NW	1	15–20	7a
	2 fault terminations	2	NW	1	19–20	7a
	Fault termination and fissure	4	NW	1	69	7b
	2 fault terminations	1	SE	1	48–50	–
	Total (probable)	11				
Coa-2	Fault termination	1	NW	2	58	–
	2 fault terminations	1	NW	2	64	–
	Fault termination	2	SE	2	47	–
	2 fault terminations	1	SE	2	49	–
	Fault termination	2	NW	2	29	7c
	Fault termination	1	SE	2	25	–
	Fault termination	1	SE	2	15	–
	Fault termination	1	SE	2	17	–
	Liquefaction features	3	SE	2	35–42	7d
	Total (probable)	13				
Coa-3	Thickness change of unit 3L	3	NW	1–3	18–21	8; 6a
	Total (possible)	3				
Coa-4	Fault termination and draped scarp	3	NW	3	18	9a
	2 fault terminations	2	NW	2	12–13	–
	Fault termination and possible colluvial wedge	3	SE	3	16–18	9b
	Total (probable)	8				
Coa-5	Fault termination and deformation contrast	4	SE	5	27	10
	Fault termination, draped scarp	3	NW	3	13–15	–
	Total (probable due to rank 4 evidence)	7				
Coa-6	Possible fault terminations	1	SE	4	50–52	–
	Possible fault terminations	1	SE	5	16	11a
	Possible fault termination	1	NW	5	16–17	–
	Possible fault termination	1	NW	5	31	–
	Possible colluvial wedge	3	SE	4–5	28–29	11b
	Total (possible)	7				
Coa-7	Fault termination	1	SE	4	10	–
	Fault termination	1	SE	4	12	–
	Fault termination	1	SE	4	13	–
	Fault termination	2	NW	4	55	12
	Broad thickening of unit 5L	3	both	4	30–50	6a
	Total (probable)	8				
Coa-8+	Fissure	3	NW	5	8	13
	Total (possible)	3				

amounts of section have been removed by erosion, such as those labeled 4/5 on Fig. 6a).

Coa-1. An earthquake probably occurred in the very latest stages of deposition of unit 1L, perhaps when the shoreline was located in the vicinity of this site (having already receded from the 12 m highstand). The best evidence for this earthquake is a slump deposit, formed when the upper half of the latest lake deposit slid northeastward along a detachment (Fig. 7a). Given the very gentle slope of the deposit, it seems highly likely that this deformation was seismically driven. The highly ductile nature of the deformation indicates that it must have occurred while the sediments were water-saturated, but the lack of subsequent lacustrine deposition indicates that the lake level must have dropped below this site very soon after the earthquake occurred. The toe of the slump also overrides some sand that appears to be aeolian, suggesting that the adjacent land surface was dry. Two strands of the SWFZ terminate below this slump (meters 19–20), while another continues all the way to the surface through unit 1S (meter 15), the latter likely a result of subsequent interseismic creep. In the northeast fault zone (northwest wall), faulting offsets the latest lake deposit, forming a fissure that is filled, at least in part, by the overlying sand (Fig. 7b). On the opposite wall, two fault strands offset the latest lake but are truncated by the overlying erosional unconformity. All these features are best explained if an earthquake occurred in a near-shore environment.

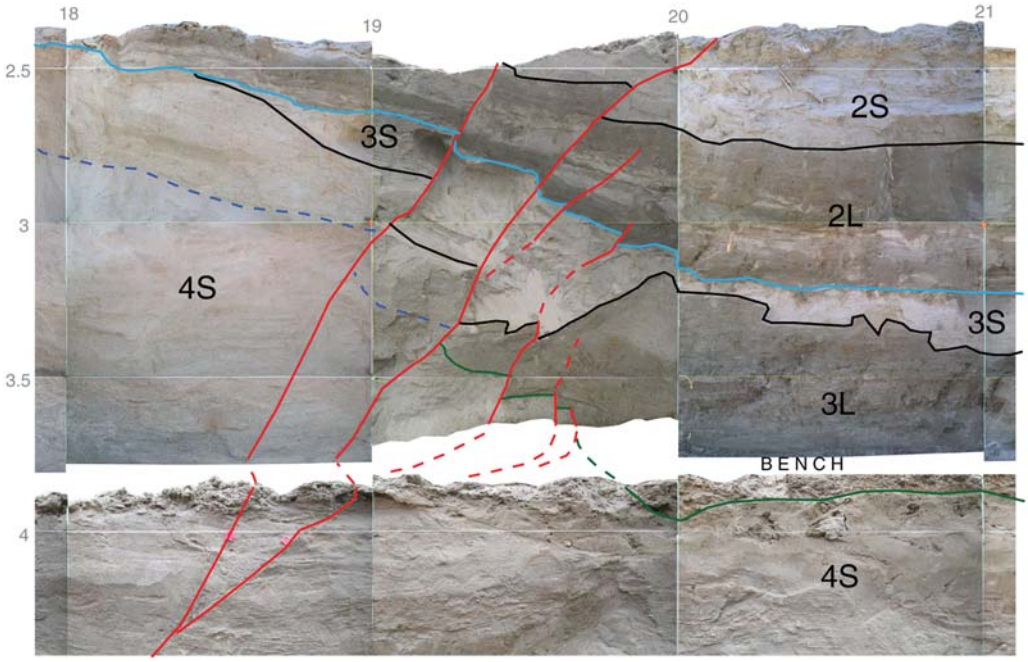

Figure 8. Evidence for Coa-3. Northwest wall, risers 2–3, meters 18–21 showing that unit 3L appears to pinch out and is not preserved on the upthrown side of the fault (the dashed blue line marks an internal contact within 4S). The top of unit 4S is vertically offset more than 2 m, while unit 2L is offset only ~75 cm and does not significantly change thickness. This suggests that an earthquake during the deposition of 3L produced accommodation space, causing 3L to form a significantly thicker deposit in the depression. The two minor fault strands that appear to terminate within 3L near the center of this view may be related to this earthquake. However, it is clear that the top of 4S (which 3L was deposited upon) was not a flat, smooth surface, so it may be possible to explain the evidence via erosional topography and lateral offset during the later earthquakes Coa-1 and 2. Based on this evidence Coa-3 is evaluated as a possible (rather than probable) earthquake.

Coa-2. An earthquake probably occurred during the deposition of the upper part of unit 2L. Six fault strands in the northeast fault zone, two fault strands in the central fault zone, and two fractures in the SWFZ terminate in layer 2La, leaving the upper surface of the lake deposit unfaulted. The locations of these terminations are given in Table 1; the best example is shown in Figure 7c. This earthquake must have occurred shortly before a drying phase of the lake, perhaps preceding desiccation of the site by a few decades. On the southeast wall of the trench, sandy layers within the second youngest lake deposits (layer 2Lb) form swooping flame structures, almost certainly a result of liquefaction (Fig. 7d). Because the layers must have been water-saturated and close to the ground surface (but confined) for this type of deformation to occur, this was most likely caused by an earthquake that occurred during the later stages of 2L deposition, consistent with the upward termination evidence.

Coa-3. An earthquake may have occurred during the deposition of unit 3L, though the exact earthquake horizon is unclear. On the northwest wall, unit 3L gradually thickens southwestward from meter 54 to meter 20 (see Fig. 6a), at which point it appears to pinch out against unit 4S just northeast of the main SWFZ. There are some minor fault strands that appear to terminate within unit 3L near this feature (Fig. 8). On the southwest side of this fault zone, unit 3L is very thin or absent, whereas unit 2L above maintains a significant thickness on both sides of the fault zone (see Fig. 6a). The gradually tapering thickness of 3L could have been produced by the sediments of 3L accumulating in accommodation space produced by a recent fault offset. There are no other recognized fault strands that terminate within unit 3L, so it may be possible to explain the evidence for Coa-3 nontectonically via erosional topography and lateral offset (during Coa-1 and -2) of layers with heterogeneous thickness. The elevation of the top of unit 4S varies considerably along the strike of the fault (on opposing walls), indicating that there was significant erosional topography on this surface prior to the deposition of unit 3L. Therefore, Coa-3 is classified as a possible earthquake because the evidence for it is less direct.

Coa-4. An earthquake probably occurred when unit 4Sd, near the middle of the thick subaerial deposit 4S, was at the ground surface. Three fault strands in the SWFZ terminate in this unit. A set of laminar sand beds overlie the terminus of one fault and pinch out, suggesting that this sediment filled in a low area adjacent to a scarp (Fig. 9a). This earthquake horizon is bracketed between two thin organic layers within layer 4S, the lower one (4Se) faulted and the upper one (4Sc) undisturbed. Additionally, there is a zone of very loose and disorganized sediment in the upper half of layer 4S where it encounters the SWFZ on the southeast wall (Fig. 9b). The bench riser wall below exposes a fault with ~70 cm of reverse separation on unit 4L, suggesting that the zone of loose sediment may be a colluvial wedge related to the

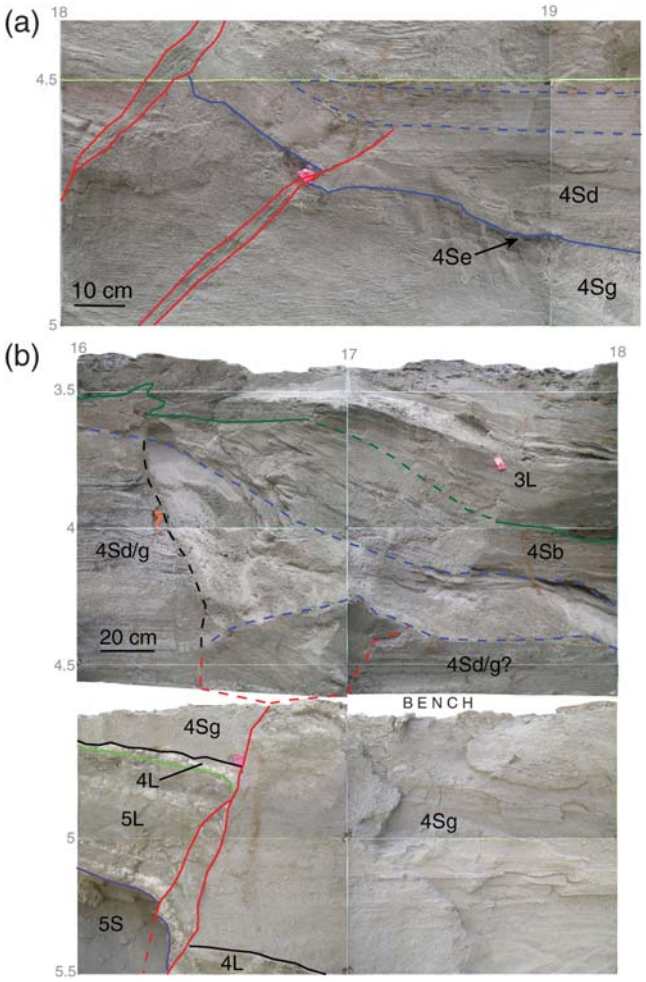

Figure 9. Evidence for Coa-4. (a) Northwest wall, riser 3, meters 18–19 showing a fault termination within unit 4S draped by a set of fine laminar beds (outlined by dashed blue lines), which appear to pinch against a paleoscarp. (b) Southeast wall, risers 3–4, meters 16–18 (reversed) showing probable collapse scarp (dashed black line) and colluvial wedge of loose sand (between dashed blue lines) in unit 4S above a fault that offsets the base of 4S by 70 cm.

collapse of an overhanging scarp. This scenario places the earthquake horizon about halfway up the wall, above which the upper part of 4S and 3L drape over the scarp and wedge. However, it is also possible that the wedge of loose sediment was formed by the cutting and filling of a channel that eroded away the upper part of the fault, in which case the original earthquake horizon is not preserved. In either case the fault terminates within unit 4S.

Coa-5. An earthquake probably occurred when the organic-rich soil developed at the top of the subaerial unit 5S was at the ground surface. Near the base of the section exposed in the central fault zone, unit 5S and the organic soil are strongly folded and unconformably overlain by undeformed beds of unit 4L (Fig. 10). This earthquake probably created the topographic depression that was then filled by the thick sequence of lake sediments that make up unit

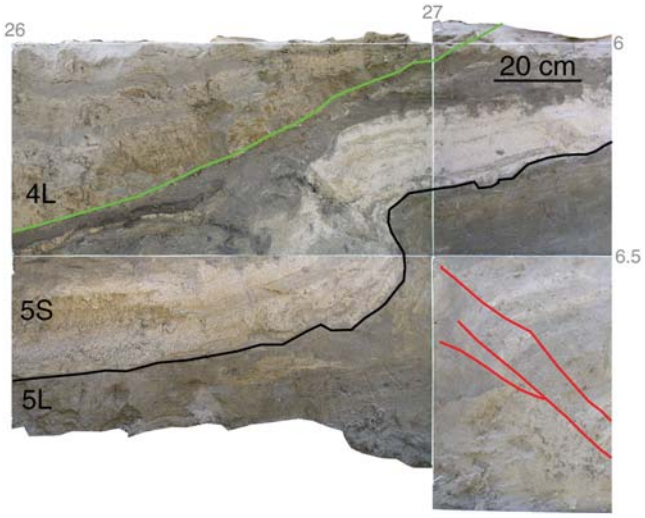

Figure 10. Evidence for Coa-5. Southeast wall, riser 5, meters 26–27 (reversed) showing folded and offset units 5S and 5L unconformably overlain by the undeformed clay and silt layers of unit 4L.

4L; these deposits thin dramatically at the edges of the deep depression. The base of unit 4L also drapes a small scarp at a fault terminus in the SWFZ.

Coa-6. There is some evidence that an earthquake occurred during deposition of unit 5L, though much of this evidence may actually be related to Coa-5. Several minor fault strands seem to terminate within the unit, but the positions of the excavation benches, disruption of bedding in the fault zones, and the obliquity of the faults to the exposed surface make it difficult to determine exactly how high these faults propagate. For instance, fault strands in the SWFZ shown in Figure 11a clearly offset the base of 5L by 20 cm, but it is difficult to determine whether the bioturbated contact between 5L and 5S is offset. Along the same trend is a fault that offsets 4L by 2 cm, but it is unclear how this fault connects to those below (if at all). The upper fault may simply be a later, unconnected minor fracture. There are similarly ambiguous fault terminations exposed in three other locations (see Table 1). There is also a possible colluvial wedge composed of sediment from 5L in the central fault zone (Fig. 11b). At least part of the wedge appears to be overlain by 5S, suggesting that the wedge formed prior to Coa-5 that deforms 5S. Bioturbation of 5S and later faulting make it unclear whether 5S is also deformed as part of the wedge, so it is conceivable that the wedge formed during Coa-5. If Coa-6 is not a true earthquake, most of the evidence for it should instead be attributed to Coa-5, considerably increasing the confidence rank of the later earthquake.

Coa-7. An earthquake probably occurred when the subaerial unit 6S was at the ground surface. Three fault strands in the southwest zone cut the base of the loose beach sand (layer 6S southwest) but do not extend into 5L. The beach

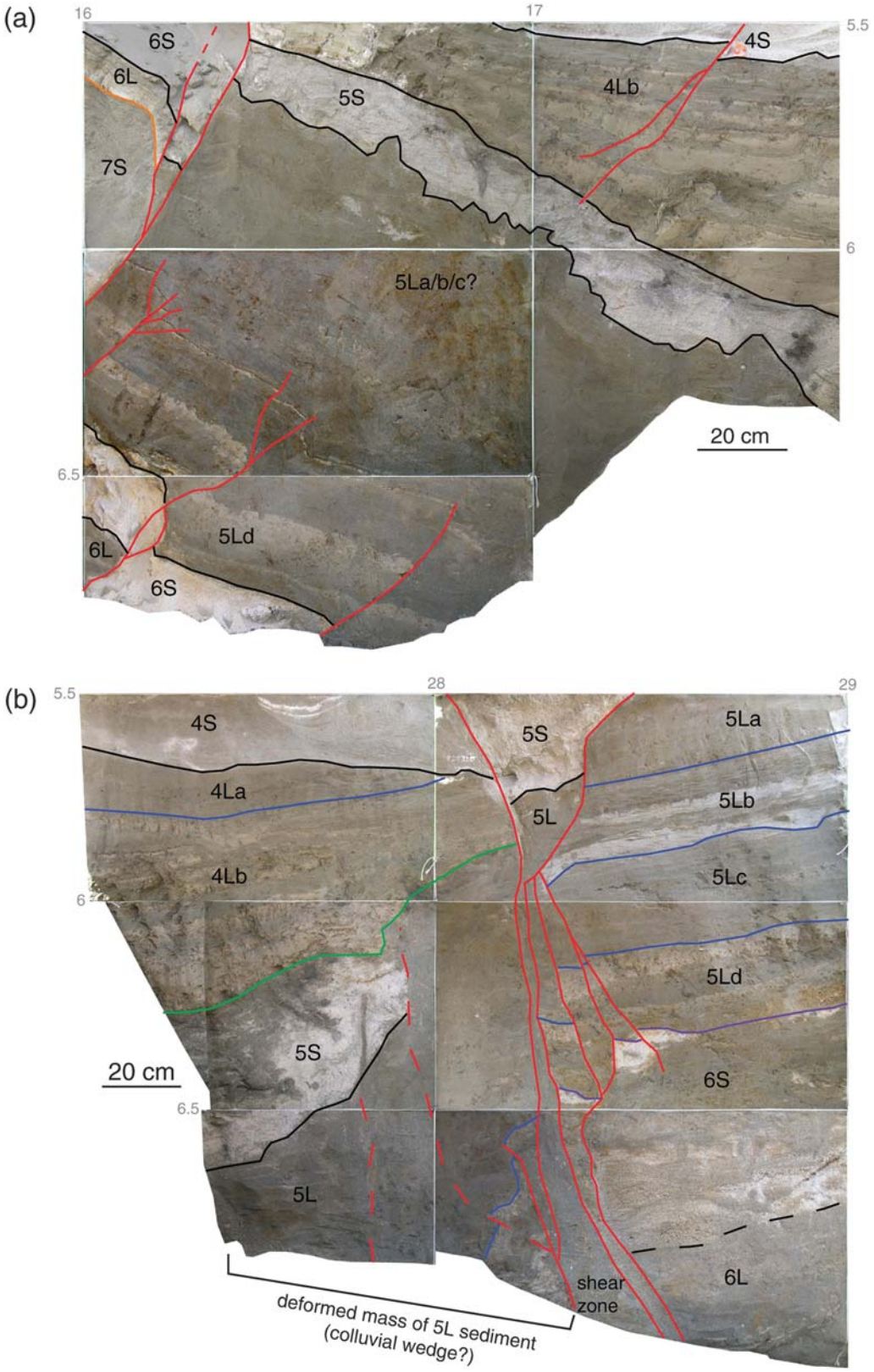

Figure 11. Evidence for Coa-6. (a) Southeast wall, risers 4–5, meters 16–17 (reversed) showing possible fault terminations within unit 5L. (b) Southeast wall, risers 4–5, meter 28–29 (reversed) showing possible colluvial wedge of material from unit 5L, suggesting scarp formation during deposition of 5L. 5S appears to overlie the lower part of the wedge, but it is absent over the highest part of the wedge.

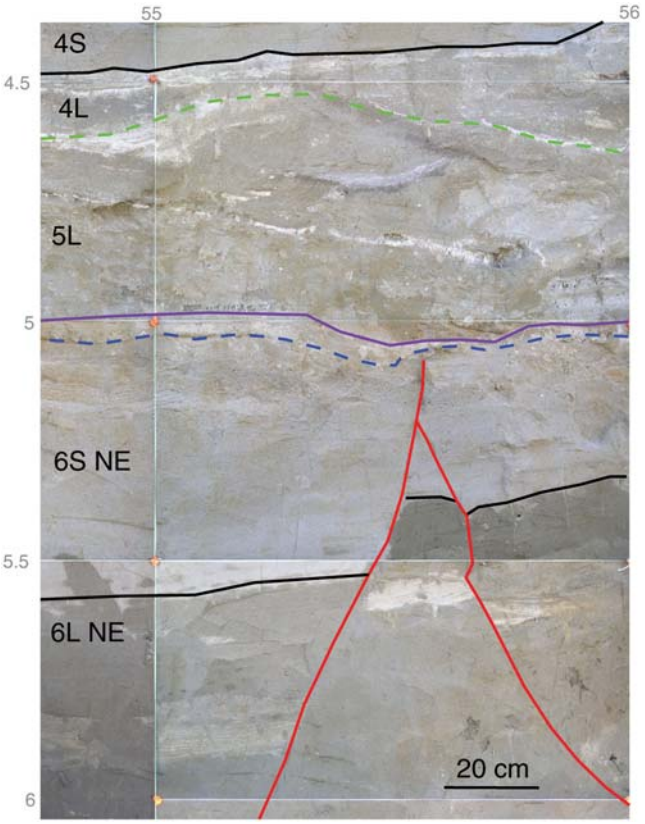

Figure 12. Evidence for Coa-7. Northwest wall, riser 4, meters 55–56 showing faults displacing units 6L NE and 6S NE, but not the upper sand layer of 6S nor the base of 5L.

sand is absent in the northeast fault zone, but one fault strand terminates in the fine-grained subaerial unit below 5L (Fig. 12). Further supporting Coa-7, unit 5L thickens from 40 cm to 120 cm over the 30 m width of the shallow depression (see Fig. 6). It is below the trench floor in the 10-m-wide deep depression, but is presumably thickened to an even greater extent there. This thickening may reflect down-dropping of the depression block prior to Lake 5 deposition.

Coa-8+. An earthquake may have occurred during the early stages of deposition of the thick fluvial unit 7S. A fissure at the very base of the trench exposure cut through unit 7L southwest and the very lowest part of 7S southwest and filled with sand from 7S southwest (Fig. 13). This feature is ranked 3 rather than 4 because it was difficult to see whether there was a fault at the root of the fissure. It is possible that one or more other earthquakes occurred between this event and Coa-7, because there appears to have been substantial erosion between the deposition of units 7L southwest and 7S southwest. Deposits of this age were not exposed in the structural depression, and due to the thickness of overlying deposits could be meters below the base of the exposure.

Eastern Trench Earthquake Evidence

The structure and stratigraphy exposed in the 200-meter-long eastern trench were dramatically different from those in the central trench. In the eastern trench, two fault zones were exposed: (1) the main fault zone that underlies the surface

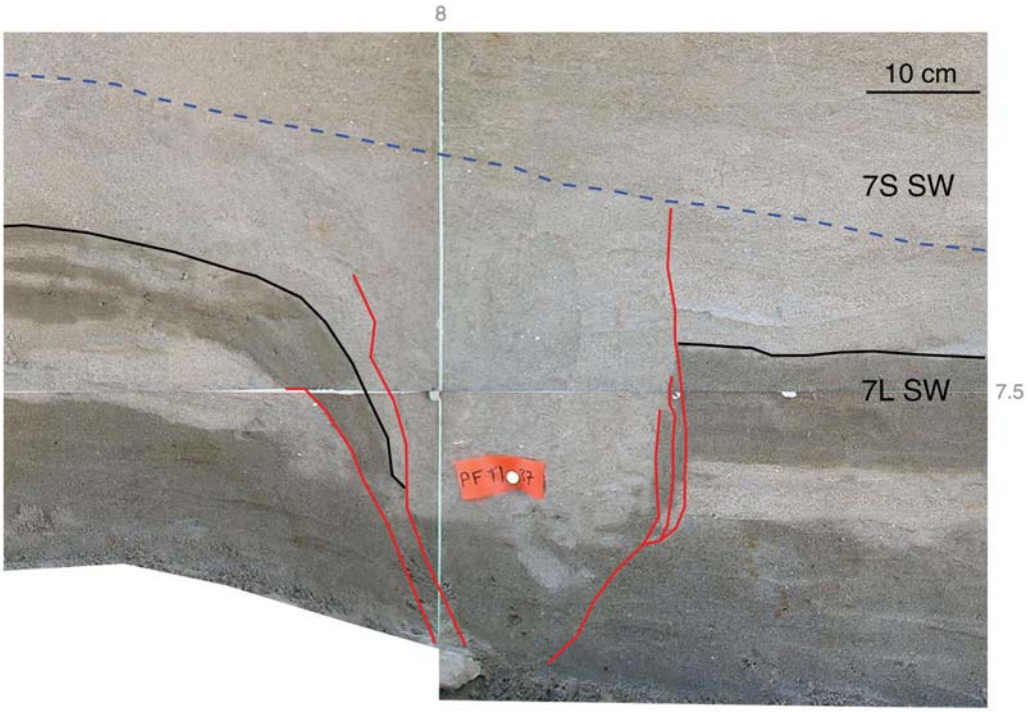

Figure 13. Evidence for Coa-8+. Northwest wall, riser 5, meter 8 showing a fissure in unit 7L southwest filled with sand from unit 7S southwest above. Only the lowermost part of 7S is faulted. Orange tag shows the location of sample Nb5m8A-sh1.

scarp and vegetation lineament and is along strike from the southwest and central fault zones exposed in the central trench, and (2) an apparently minor fault zone near the northeast end of the trench (see Fig. 3). The extensive erosion between lacustrine intervals made it difficult to correlate the stratigraphy between the trenches and to precisely identify earthquake horizons. Because no fault-parallel trenches were available for study, it was necessary to rely on radiocarbon ages to guide our correlations of stratigraphic units between the trenches; carbon samples were unfortunately relatively scarce in the eastern trench exposures. An organic layer associated with the youngest lake in the exposed section (in the vicinity of the minor northern fault zone) yields a date of 390 ± 35 ^{14}C-yr B.P., suggesting that deposits from the most recent lake have been entirely removed or were never deposited at that location. If our correlation is correct, there is some evidence for Coa-3, -4, and -5 (Philibosian *et al.*, 2009), but due to the correlation uncertainties this evidence does not provide much additional confidence in our earthquake chronology.

Radiocarbon Dating

We obtained 82 radiocarbon dates from 61 samples, 49 from the central trench and 12 from the eastern trench (Table 2). See Philibosian *et al.* (2009) for exact sample locations. Sediment blocks containing organic layers were collected at 15 of these locations, while detrital charcoal and/or lacustrine mollusk shells were collected at the others. To isolate the carbon, each organic layer was dissected to remove potentially younger roots and as much nonorganic sediment as possible. The carbon from these organic-rich layers is in the form of black, amorphous, spongy clumps. With essentially none of the material's original structure preserved, it is difficult to determine whether it is decomposed plant matter or burnt material from a local fire. In some places these layers had a ruddy tinge, indicating oxidation of sediment that is often observed following a fire, so we infer that these layers are probably burn horizons.

We applied chemical treatments to the charcoal and soil samples prior to dating them via accelerator mass spectrometry (AMS) carbon-14 analysis. Charcoal samples were given the standard acid-alkali-acid (AAA) chemical pretreatment to remove atmospheric carbon and humic acids. For each sample of the organic-rich layers, humic acid dissolved in the first base wash solution was precipitated and dated separately from the AAA fraction. Humic acid, being soluble in base, is usually discarded in the AAA process because it may be leached from more modern material and transported through groundwater. However, if the organic material is decomposed plant matter, the humic acid may be derived from *in situ* plant matter and thus has the potential to provide a more accurate date than an AAA-treated sample, which may contain older detrital charcoal (Scharer *et al.*, 2007). Following pretreatment, combustion to CO_2, and precipitation as graphite, the samples were dated at the Center for Accelerator Mass Spectrometry (CAMS) facility at Lawrence Livermore National Laboratory (LLNL) or at the Keck Carbon Cycle Accelerator Mass Spectrometry (KCCAMS) Laboratory at the University of California at Irvine. Dates in carbon-14 years before present (B.P.) were obtained from the $^{14}C/^{12}C$ ratio and corrected for isotopic fractionation using the $^{13}C/^{12}C$ ratio.

In a few cases we extracted charcoal and/or shells from block samples and dated those in addition to the AAA and humic fractions from the organic sediment. Both charcoal and a shell from location Nb4m44A were dated, and a lone shell was dated at location Nb5m8A because no charcoal was present. Where both occur, the shell ages are between 400 and 800 yr older than the charcoal and/or organic sediment ages from the same sample location, indicating that past waters of Lake Cahuilla contained a significant reservoir of old carbon. We found no macrofossils other than roots, which are likely young throughout the section because roots from an old organic sediment sample (AAA date of 960 ± 30 B.P.) yielded a modern age.

Earthquake Chronology Determination Using OxCal

We used the OxCal v. 4.1 program (Bronk Ramsey, 2009) to convert ^{14}C yr B.P. into calendar years B.C./A.D. based on the history of atmospheric ^{14}C concentration, using the IntCal04 calibration curve (Reimer *et al.*, 2004). The OxCal program convolves the uncertainties, producing a probability density function (PDF) for each date. We applied additional stratigraphic constraints to trim the PDFs: samples from the same stratigraphic layer are grouped as Phases in OxCal in which no internal stratigraphic constraints are applied, and the known stratigraphic relationships between samples and groups of samples were enforced by an ordered Sequence. Earthquake ages are determined in OxCal by calculating PDFs that are statistically consistent with the radiocarbon age PDFs, using the Date functionality.

Because of fluctuations in atmospheric ^{14}C concentration since the dawn of the industrial revolution, measurements of <200 ^{14}C-yr B.P. generally match multiple calendar date ranges. Thus, it is prudent to consider historical observations in order to better constrain the ages of the youngest deposits. Early expeditions through the region by Europeans provide useful historical constraints on the timing of the two most recent fillings of Lake Cahuilla (summarized in Lippincott, 2007). The first European expedition to pass through the Salton Trough was that of Anza in 1774. Records from this journey make no mention of a lake, but it is possible that a relatively small saline lake (unworthy of mention) may have been present at the time. Frequent subsequent expeditions and the eventual settlement of the region preclude the possibility that Lake Cahuilla filled after 1774. It has been estimated that once cut off from Colorado River input, Lake Cahuilla would require 60 yr to desiccate entirely (Waters, 1983; Sieh and Williams, 1990), so in order for it to have been dry by the time of the Anza expedition a full lake

Table 2
Ages of Carbon Samples in Stratigraphic Order

Sample Name*†	^{14}C age	±	Layer‡§	
Central Trench Samples				
Nb1m45A-c	125	20	1S	–
Nb1m51A-c	175	15	1S	–
Sb1m44A-c	210	15	1S	–
Nb1m57A-b-hum	*Modern*	–	*1La*	*X*
Nb1m57A-b-AAA	*200*	*35*	*1La*	–
Nb1m57A-c	*260*	*40*	*1La*	–
Nb1m22A-c	105	20	1Lb	X2
Sb2m26B-c	545	20	2S	X
Sb1m55A-c	590	15	2S	X
Sb2m34A-c	645	25	2S	X
Nb2m51A-c	485	15	2La	X1
Sb2m26C-c	520	20	2La	X1
Sb1m52A-c	715	20	2La	X
Sb2m26A-c	385	35	2Lb	X2
Nb2m36A-c	400	30	2Lb	X2
Sb3m45A-c	310	15	2Ld	–
Sb2m10A-c	335	15	2Ld	–
Sb3m44A-c	335	20	2Ld	–
Sb2m10B-c	360	25	2Ld	–
Sb3m48A-c	380	15	2Ld	–
Sb2m4A-c	670	15	2Ld	X
Sb3m59A-c	435	35	3L	–
Nb2m30A-b-hum	**545**	**40**	**3L**	**–**
Nb2m30A-b-AAA	**585**	**30**	**3L**	**–**
Nb2m44A-b-AAA	*665*	*30*	*3L*	–
Nb2m44A-b-hum	*700*	*30*	*3L*	*X1*
Nb3m41A-b-hum	**610**	**30**	**4Sc**	**–**
Nb3m41A-b-AAA	**645**	**30**	**4Sc**	**–**
Nb3m20A-b-AAA	*700*	*30*	*4Se*	–
Nb3m20A-b-hum	*705*	*35*	*4Se*	–
Nb4m28B-c	815	35	4Sf	–
Sb3m4B-b-hum	915	15	4Sg	X2
Sb4m26A-c	890	15	4La	–
Sb4m27B-c	960	15	4La	–
Sb4m27A-c	980	15	4La	X1
Sb3m36B-c	1075	15	4La	X
Sb3m49A-b-hum	**910**	**20**	**5S**	**–**
Sb3m49A-b-AAA	**915**	**20**	**5S**	**–**
Nb5m28B-b-AAA	*935*	*30*	*5S*	–
Nb5m28B-b-hum	*955*	*30*	*5S*	–
Sb4m49B-b-hum	**965**	**30**	**5S**	**–**
Sb4m49B-b-AAA	**1030**	**35**	**5S**	**–**
Nb3m65B-b-AAA	*985*	*30*	*5S*	–
Nb3m65B-b-hum	*995*	*35*	*5S*	–
Nb3m59A-b-hum	**1065**	**40**	**5S**	**–**
Nb3m59A-b-AAA	**1095**	**35**	**5S**	**X1**
Nb3m59A-c	**1230**	**80**	**5S**	**X**
Nb4m44A-c	*1185*	*40*	*5Lc*	*X1*
Nb4m44A-sh1	*1550*	*30*	*5Lc*	*X*
Sb3m7A-c	955	30	5Ld	X2
Sb3m11A-c	1075	15	5Ld	–
Sb3m3B-c	1095	20	5Ld	–
Sb3m3A-c	1150	–	–	–
Sb3m4A-c	1290	20	5Ld	X
Sb4m59A-c	2885	30	6Sa NE	X
Sb3m2A-c	365	25	6La SW	X
Sb3m0B-c	1080	15	6La SW	–
Sb3m1B-c	1105	15	6La SW	–
Nb4m13B-c	1125	20	6La SW	–
Nb4m13A-c	1185	30	6Lb SW	–
Sb4m14A-c	1185	30	7S SW	–
Nb5m8A-sh1	2975	30	7L SW	–
Eastern Trench Samples				
Main Fault Zone				
T2-Sb2-3-c	530	15	3L	–
T2-Sb2-2-c	580	15	3L	–
T2-Sb2-9-c	605	20	3L	–
T2-Sb2-17-c	610	15	3L	–
T2-Sb2-4-c	930	15	4S	–
T2-Sb2-6-c	945	15	4L	–
T2-Sb2-1-b-r	**Modern**	**–**	**5Sa**	**–**
T2-Sb2-1-b-AAA	**960**	**30**	**5Sa**	**–**
T2-Sb2-1-b-c1	**1105**	**40**	**5Sa**	**–**
T2-Sb2-1-b-sh2	**1575**	**30**	**5Sa**	**–**
T2-Sb2-1-b-sh3	**1695**	**35**	**5Sa**	**–**
T2-Sb2-1-b-sh1	**1725**	**45**	**5Sa**	**–**
T2-Sb2-8-c	1020	15	5Sb	–
T2-Sb2-7-c	1165	15	5Sc	–
T2-Sb3-1-b-hum	*1550*	*30*	*6.5L?*	–
T2-Sb3-1-b-AAA	*1570*	*35*	*6.5L?*	–
Northeastern (Secondary) Fault Zone				
T2-Sb1-1-b-hum	**390**	**35**	**2L?**	**–**
T2-Sb1-1-b-AAA	**450**	**30**	**2L?**	**–**
T2-Sb2-14-b-AAA	*1080*	*30*	*5L?*	–
T2-Sb2-14-b-hum	*1115*	*30*	*5L?*	–

*Sample nomenclature designates northwest or southeast wall, bench riser number (1 is at the top), and meter number (from the southwest end of the logged exposures). The final capital letter is used to distinguish between multiple samples in a given wall-riser-meter. In the eastern trench, samples are numbered sequentially on each bench riser. The last part of the sample name denotes the sample type:

b-AAA: bulk sediment AAA fraction
b-hum: bulk sediment humic acid
c: charcoal
r: roots
sh1: clam shell
sh2: helmet shell
sh3: turritella shell

†Each bold or italicized group of dates was obtained from different portions of the same sample.

‡Samples followed by X were judged to be stratigraphically inconsistent and were excluded from the final analysis; X numbers indicate the OxCal model refinement step at which the sample was removed.

§Question marks indicate that the layer assignment is uncertain.

must have begun to evaporate by 1715 at the latest. If a small saline lake was present, desiccation may have begun a few years later, but Father Kino's earlier expedition established that the Colorado River was flowing into the Gulf of California in 1702 (Lippincott, 2007). It is possible that the river was briefly diverted back into the Salton Trough after Kino's expedition, but the most likely explanation is that the most recent Colorado River input to the lake was prior to A.D. 1702. Earlier expeditions (discussed in the following text) may provide additional information, but were not used to constrain the carbon-14 dates. Our OxCal model includes a historical razor at A.D. 1710 within the layer 1S phase, adding a conservative estimate of the time it would have taken for the lake level to drop from the 12-meter-

elevation shoreline past the Coachella site (more likely only a few years based on estimated evaporation rates of 1–2 m/yr). Because the most recent earthquake probably occurred before the lake receded from this location, this historical razor places a pre-1710 bound on the age of Coa-1 as well as all the sample ages below layer 1S.

Because correlations of deposits between the two trenches can only be made based on radiocarbon age, only samples from the central trench were used in the OxCal model to determine the ages of paleoearthquakes. Figure 14 shows the 62 dates from the central trench grouped by source layer (excluding the modern ages and the much older shell ages). Clearly some of these detrital charcoal samples are well above the age-depth trend and thus are much older than the layers in which they were deposited. One sample (Sb3m2A-c) is so young compared with many other samples that it must have been contaminated by younger carbon, either by groundwater or during the sample pretreatment process, or been mixed into the older layer through bioturbation. The modern humic acid age (Nb1m57A-b-hum), the Nb4m44A shell age, the inconsistently young charcoal age, and nine inconsistently old detrital charcoal ages were excluded from the initial OxCal analysis.

OxCal calculates several indices that represent how well the model fits the data. For each date, the individual agreement index represents the likelihood of obtaining that measurement assuming the model is correct. The model agreement index represents the likelihood that the model is true given all of the data, and the convergence integral represents how well the Monte Carlo analysis has represented the full range of possible models. In general, the agreement indices should be $>60\%$ and the convergence integral $>95\%$ for the model to be acceptable. All models were run until the convergence integral reached 95%, so we can be confident that the model space was adequately explored in all cases. The initial model, containing 50 dates, had so many samples with low individual agreement indices that the model agreement index was 0%. We twice refined this model, removing two additional samples that appeared inconsistently young and nine that were inconsistently old. (See Philibosian, 2007 for the initial and intermediate OxCal models.) Ultimately, about 40% of the dates (1 shell, 4 possibly contaminated or bioturbated samples, and 18 detrital samples) were determined to be inconsistent with the model. The percentage of stratigraphically consistent dates compares favorably with many other recent paleoseismic sites, dated largely by detrital material, where it has often been necessary to exclude more than half of the sample dates (e.g., Fumal, Rymer, and Seitz, 2002).

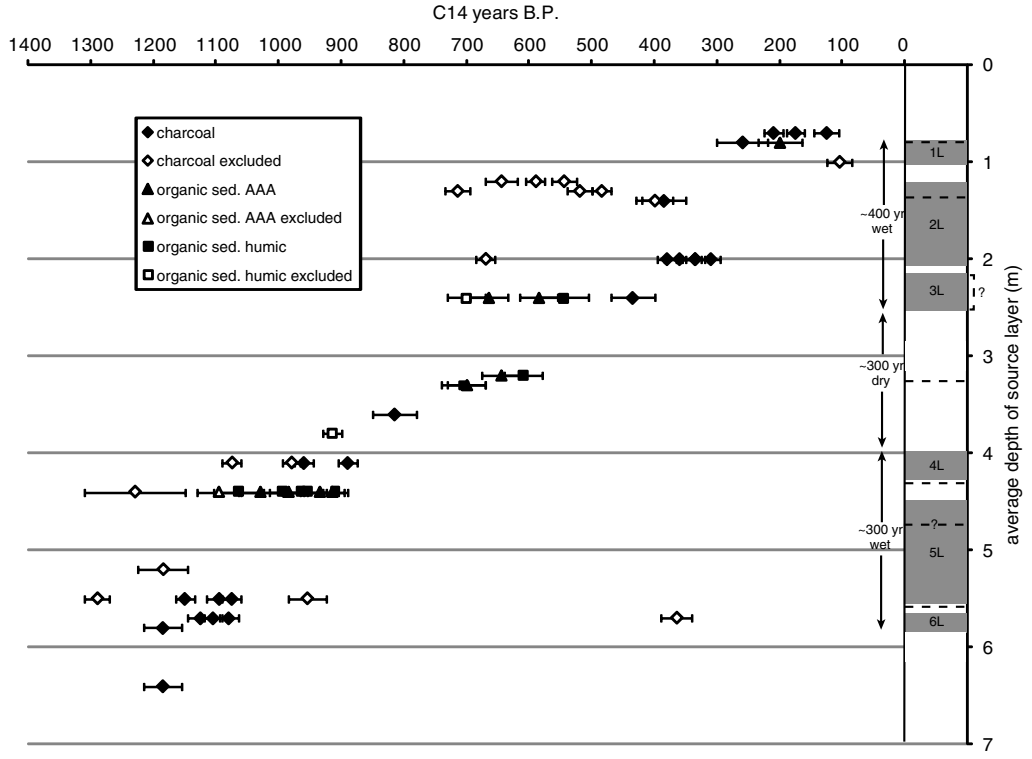

Figure 14. Stratigraphic and age distribution of dated samples from the central trench (excluding modern-aged samples and shells). Samples are plotted using the average depth of their source layer (according to the generalized stratigraphic column shown in Fig. 5). Lacustrine intervals are indicated by gray bars and earthquake horizons by heavy dashed lines. Note that while there are six distinct lacustrine intervals, they appear to be grouped into two longer mostly wet time periods during which the lake basin probably did not desiccate completely. Samples with empty symbols were excluded from the final OxCal model due to stratigraphic inconsistency once converted to calendar years.

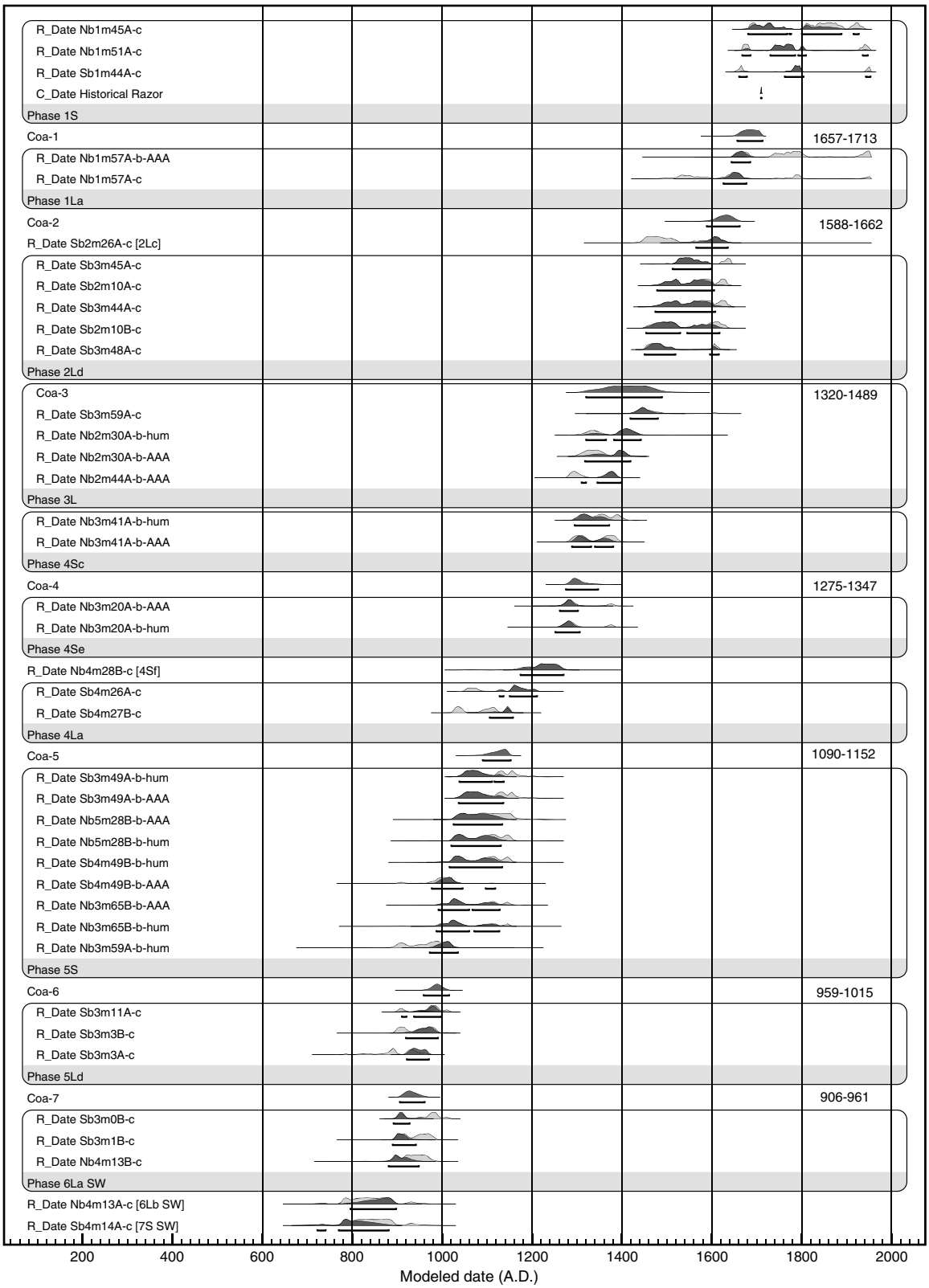

Figure 15. Final OxCal model for the central trench ages showing calibrated age distributions (open curves) and ordering-constrained distributions (shaded) with 95.4% confidence intervals (horizontal brackets). All samples have agreement indices $> 70\%$ and the model agreement index is 104%. The modeled age interval (in calendar years A.D.) for each earthquake is shown at right.

Table 3
Best Estimates (to the Nearest Decade) and 95% Confidence Ranges of Earthquake Dates*

Earthquake	Year	95% Confidence Range
Coa-1	1690	1657–1713
Coa-2	1630	1588–1662
Coa-3 (poss.)	1420	1320–1489
Coa-4	1300	1275–1347
Coa-5	1140	1090–1152
Coa-6 (poss.)	990	959–1015
Coa-7	930	906–961
Coa-8+ (poss.)	–	1090 B.C.–A.D. 784

*Dates are in calendar years A.D. unless otherwise specified.

The final model has an agreement index of 104% with individual agreement indices > 70% for all samples (Fig. 15). Based on this model, we infer that five probable and two possible earthquakes expressed in the Coachella exposures occurred after A.D. 800, in the time intervals A.D. 906–961, 959–1015 (possible), 1090–1152, 1275–1347, 1320–1489 (possible), 1588–1662, and 1657–1713 (Table 3, Fig. 16). The PDF for the poorly bracketed eighth event is essentially flat within its large interval (see fig. 23 of Philibosian, 2007), so no best estimate is given. Because the evidence for this earthquake is a fissure in layer 7L southwest filled with likely subaerial material related to the early stages of deposition of 7S southwest, the earthquake probably occurred toward the more recent end of the interval between 1095 B.C. and A.D. 784. The shell that provides the early bound on the date of this event is most likely reworked from unit 7L southwest, and due to the reservoir effect is probably hundreds of years younger than its radiocarbon age suggests.

Average earthquake recurrence intervals are often calculated by dividing the average single-earthquake displacement by the fault slip rate. However, neither of these parameters is well-characterized for this section of the SAF (see Fumal, Rymer, and Seitz, 2002; Fialko, 2006; van der Woerd *et al.*, 2006; Behr *et al.*, 2010), so the only reliable way to calculate recurrence interval is via paleoseismological earthquake chronologies such as ours. Our estimated average earthquake recurrence interval varies depending on the calculation method (Table 4). Using only the closed earthquake intervals in the chronology, the average recurrence interval can be calculated to lie between 116 and 202 yr, depending on the number of earthquakes. However, the current ~300-yr open interval is longer than most of the closed intervals, and its inclusion in the calculations raises the calculated range to 150–221 yr. Without the open interval, the calculated average recurrence interval is almost certainly biased short, so the latter range is probably closer to the true mean. Including the open interval, assuming that there have been six earthquakes, and using the best-estimate age of Coa-7, the best-estimate average recurrence interval is 180 yr.

Comparison with Other Sites and Implications for Rupture Extent and Magnitude

Figure 17 compares the Coachella earthquake chronology with other paleoseismic sites on the southern San Andreas fault at Indio (Sieh, 1986); Thousand Palms Oasis (TP: Fumal, Rymer, and Seitz, 2002); Burro Flats (BF: Yule and Sieh, 2001; Yule, personal commun., 2004; Yule *et al.*, 2006); Plunge Creek (PlC: McGill *et al.*, 2002); Pitman Canyon (PiC: Seitz *et al.*, 1997); Wrightwood (WW: Biasi *et al.*, 2002; Fumal, Weldon, *et al.*, 2002; Weldon *et al.*, 2002; Weldon *et al.*, 2004); and Pallett Creek (PaC: Sieh *et al.*, 1989; Salyards *et al.*, 1992; Biasi *et al.*, 2002). Locations of these sites are shown on Figure 1b. Coa-1, Coa-3, and Coa-4 correlate reasonably well with the three most recent earthquakes at both Thousand Palms and Indio. (It should be noted that

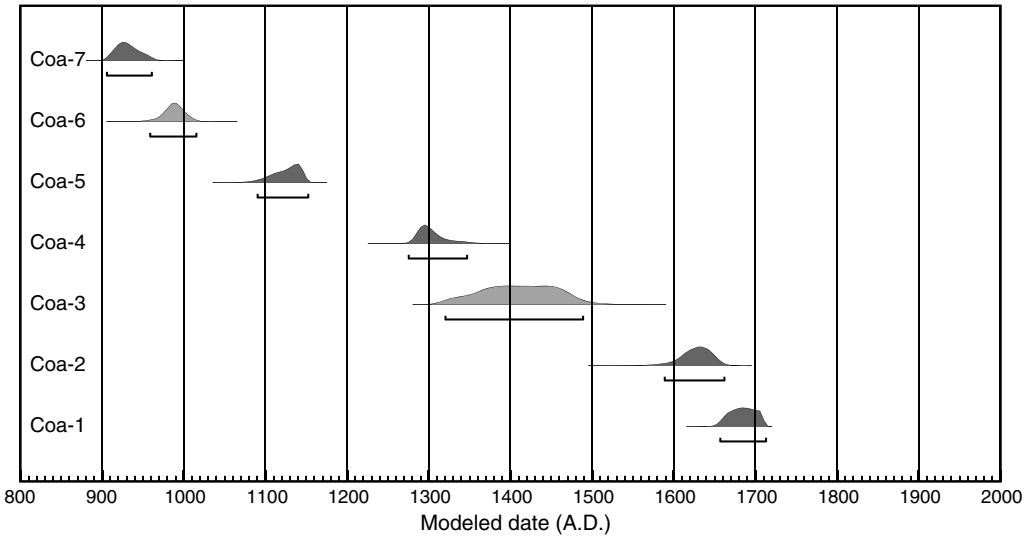

Figure 16. Probability density functions (PDFs) for the seven earthquakes recorded at the Coachella site. Probable earthquakes have darkly shaded PDFs while possible earthquakes are lightly shaded. Brackets below PDFs show 95.4% confidence intervals. Note that the current interseismic interval appears anomalously long.

Table 4
95% Confidence Ranges of Mean Earthquake Recurrence Intervals

Recurrence Intervals	Including Open Interval	Without Open Interval
5-earthquake scenario	210–221 yr	174–202 yr
7-earthquake scenario	150–158 yr	116–135 yr

similar historical constraints were applied to the most recent event at all three sites, so the several estimations of its age are not independent). However, Coa-2 does not correlate well with any of the earthquakes recorded at either Thousand Palms or Indio. The Thousand Palms site is located on the Mission Creek strand of the SAF. It is thought that in the vicinity of this site slip is being transferred from the Mission Creek strand to the Banning fault and indeed, slip-per-event at the Thousand Palms site is small, averaging only about 50 cm (Fumal, Rymer, and Seitz, 2002). Thus, it would not be surprising that an earthquake rupture might be absent or poorly manifested and preserved at that site. Also, detailed results have not been published for the Indio site, so it is not possible to evaluate either the completeness of the stratigraphic record or quality of the earthquake evidence there. Thus, it is possible that three earthquakes occurred since A.D. 1400, but evidence for Coa-2 was not preserved at Thousand Palms or Indio. Alternatively, Coa-2 could represent the tail end of a relatively short southerly rupture that did not extend as far north as Indio. We also cannot entirely rule out the possibility that some faults that ruptured during earlier earthquakes propagated only partway to the surface during the most recent earthquake (Coa-1), leaving misleading evidence for an intervening earthquake (Coa-2) that never actually occurred. However, to the best of our ability to interpret the evidence, Coa-1 occurred within a century of Coa-2.

The correlation of Coa-5, -6, and -7 with the other chronologies is less certain. The stated uncertainty in the date of TP-4 is very large and that for Indio-4 is probably much

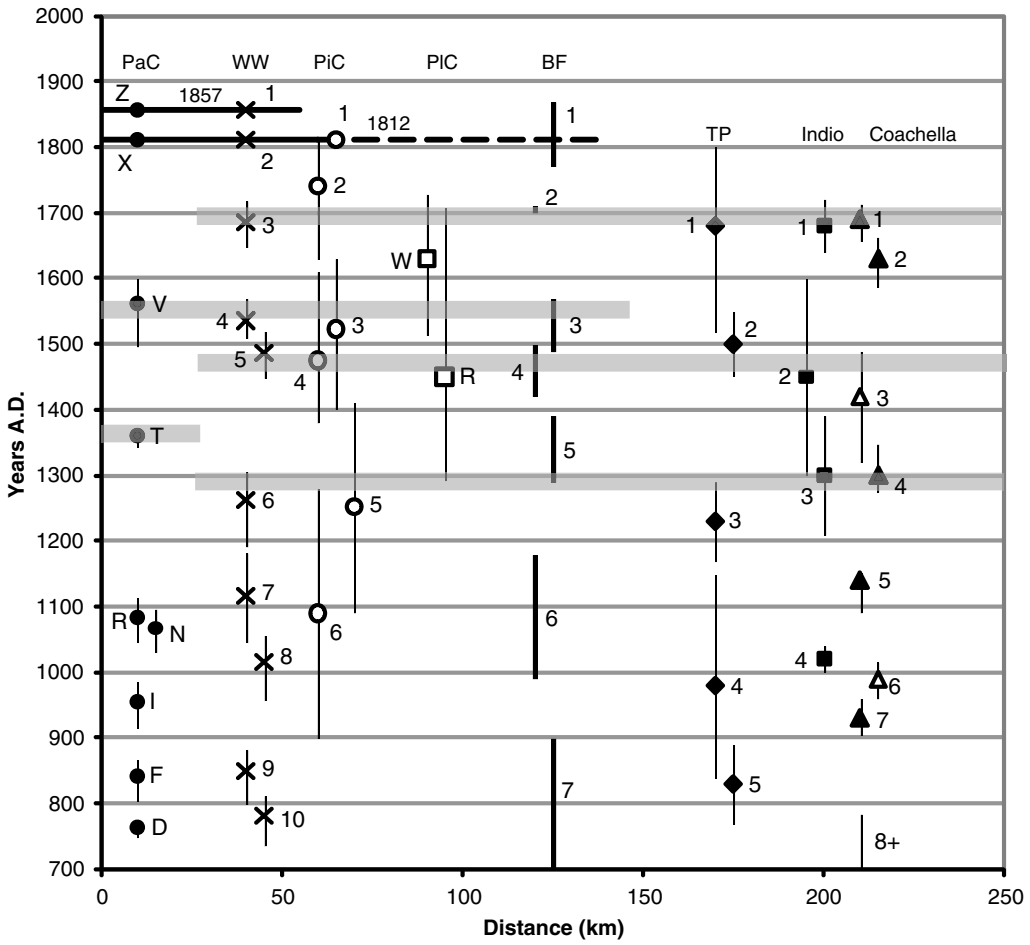

Figure 17. Earthquake chronologies from paleoseismic sites on the southern San Andreas Fault. The possible earthquakes Coa-3 and Coa-6 are shown by empty triangles. Rupture extents of the historical 1857 and 1812 earthquakes are shown by horizontal black bars. Gray bars show possible correlations between sites, delineating separate Coachella Valley and Mojave section ruptures. Site abbreviations: PaC: Pallett Creek, WW: Wrightwood, PiC: Pitman Canyon, PlC: Plunge Creek, BF: Burro Flats, TP: Thousand Palms. (Note that only age brackets, without best estimates, are available for the Burro Flats site). Sources for site chronologies are listed in the text.

smaller than stratigraphic bracketing of the event actually permits. These events could correlate with any of Coa-5, -6 or -7 at Coachella, but it seems most likely that they correlate with Coa-5, because there is an older fifth earthquake at Thousand Palms that may correlate with Coa-6 or -7. (The Indio record does not extend farther back in time than A.D. 1000). Alternatively, if TP-4 and Indio-4 correlate with Coa-6 or -7, this means Coa-5 was not recorded at either of those sites, and TP-5 was not recorded at Indio or Coachella (reasonable because it is older than the continuous section exposed at both sites). For reasons noted previously, the paleoseismic records at the Thousand Palms and Indio site may not be complete and this may account for the discrepancies in the chronologies among the sites. Importantly, all three sites are consistent with 5–7 earthquakes occurring since A.D. 800. Preliminary results from the Salt Creek site are also in agreement (Williams, 2009).

It is of particular scientific and social interest to determine the rupture length of past earthquakes on the Coachella Valley section of the SAF, because this touches on the fault segmentation issue and is related to estimating the damage potential of a future earthquake. The three Coachella Valley sites' similar histories suggest that the Coachella Valley section of the fault is usually part of a single rupture. To estimate rupture extent, we can compare the Coachella Valley chronology with those obtained at more distant sites. Earthquakes at each of the northern sites (WW-3, PiC-2, PlC-W, and BF-2) likely correlate with the most recent (late 1600s) event in the Coachella Valley. However, no event of a similar age appears in the Pallett Creek record, so it seems fair to conclude that the earthquake that occurred in ~A.D. 1690 probably ruptured the 150 kilometers of fault between Coachella and Wrightwood, but did not propagate farther northwest. The penultimate (mid-1400s) Coachella Valley rupture (manifested as Coa-3, Indio-2, and TP-2) potentially correlates with BF-4, PiC-4, and WW-5, but there is again no corresponding Pallett Creek earthquake. PaC-V does likely correlate with WW-4, PiC-3, and BF-3, suggesting that an early 1500s earthquake reruptured the fault between Wrightwood and Burro Flats, but did not extend into the Coachella Valley. (PlC-R could correlate with either the northern or the southern rupture; the Plunge Creek record is almost certainly incomplete). The third (c. 1300) Coachella Valley rupture (Coa-4, Indio-3, and TP-3) similarly potentially correlates with BF-5, PiC-5, and WW-6, but not with any Pallett Creek earthquake. These potential correlations are delineated by gray bars on Figure 17. The earlier parts of the records are more difficult to interpret in terms of regional correlations due to the lack of a clear consensus among the Coachella Valley sites.

These chronologies suggest that the Coachella Valley section of the SAF does not usually rupture with the Mojave–Carrizo Plain section. The stretch of the fault between Wrightwood and Burro Flats appears to be a transition zone that sometimes (but not necessarily always) ruptures along with the Coachella Valley or Mojave sections of the fault. While the data could be explained by a random rupture model, the good agreement between likely Coachella Valley events with Wrightwood, Pitman Canyon, and Burro Flats events (and absence of agreement with Pallett Creek events) lends support to the characteristic model. It is interesting to note that while the Coachella Valley segment ruptures separately from the Mojave–Carrizo Plain segment, there appears to be a broad transition zone between the two rather than an abrupt segment boundary, with Coachella Valley events occasionally propagating through (or starting north of) the structurally complex San Gorgonio Pass. Therefore, evidence presented here suggests that the structural knot may not pose a significant barrier to through-going rupture, and a 500- to 600-km-long rupture of the entire southern SAF is not entirely out of the question.

An additional point of interest is that the penultimate earthquake on the Imperial fault (which last ruptured completely in 1940, with rerupture of the northern section occurring in 1979) appears to have occurred during the most recent lake highstand (Thomas and Rockwell, 1996). Though available age control is far from adequate to determine the relative timing of the penultimate Imperial fault rupture and the most recent Coachella Valley SAF rupture (Coa-1), the brief duration of the most recent lake suggests that they occurred within ~50 yr of each other. It seems likely that the events were related: one earthquake could have triggered the other via stress changes, similar to the suspected triggering of the 1999 Hector Mine earthquake by the Landers earthquake 7 yr earlier (e.g., Felzer *et al.*, 2002; Kilb, 2003). Alternatively, the southernmost San Andreas fault and the Imperial fault could have ruptured in a single earthquake, though this seems somewhat unlikely given the transtensional structural complexities in the intervening Brawley seismic zone (see Fig. 1b).

Lake Chronologies

Our investigations at the Coachella site were focused on developing a paleoearthquake chronology, but our stratigraphic observations and extensive radiocarbon dating provide important data regarding the history of Lake Cahuilla. We obtain approximate dates and durations of lacustrine intervals by projecting the thickness of the lake sediment through the date-constrained sedimentation rate (Fig. 18). Note that these are durations at the 9-meter elevation mark; sites located at lower elevation are expected to record longer durations, and those at the 12-m highstand shoreline would be slightly shorter. The bottom of the basin, at an elevation of ~85 m below sea level, could have lacustrine deposition for a few decades before the lake reached the 12 m highstand, and for ~60 yr after the lake began to desiccate (Waters, 1983; Sieh and Williams, 1990). The only previously published lake sequence, from sites located at sea level (Waters, 1983; see Fig. 1b) is shown at the top of Figure 18 and is very different from the Coachella chronology. These differences cannot simply be attributed to the 9-meter difference in

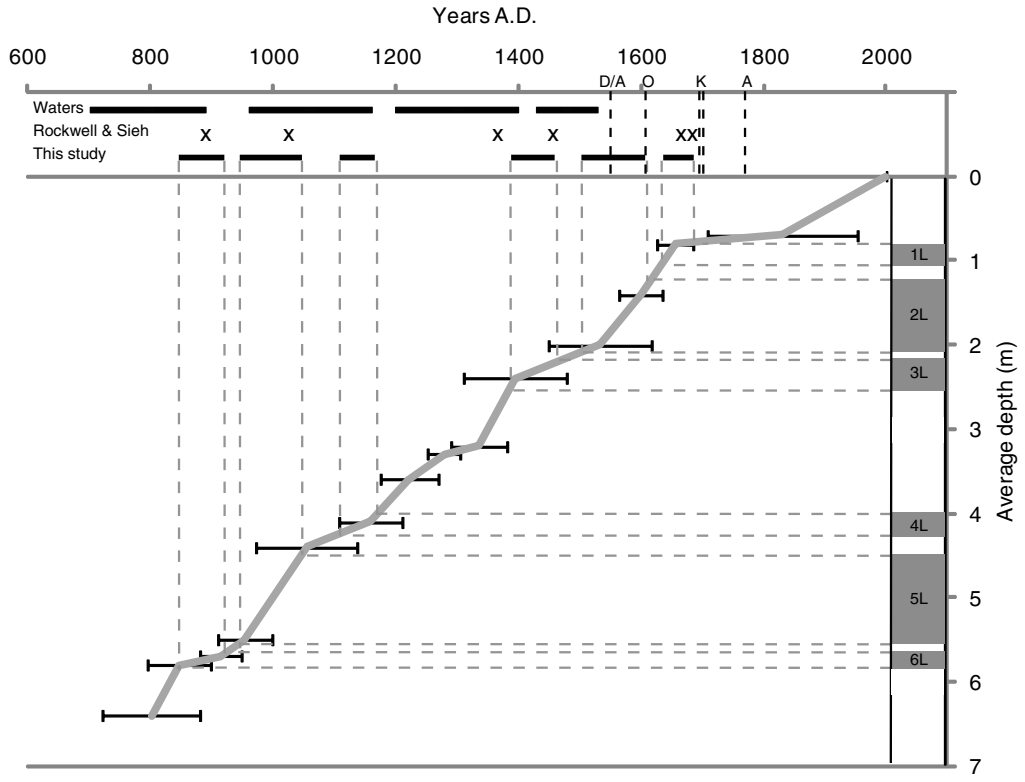

Figure 18. Approximate lake highstand chronology at the Coachella site and comparison to other Lake Cahuilla chronologies. The full 95% confidence range of the modeled ages of samples from each layer is plotted against average depth of the source layer. Lacustrine periods are projected from the depth axis to the time axis using the best-fit instantaneous sedimentation rate (heavy gray line). The resultant chronology has six distinct highstands, but these are grouped into two "mostly wet" periods. The intervals of subaerial deposition within the mostly wet periods were probably not long enough for the lake to desiccate completely. Lake durations from Waters (1983) and ages of deposits immediately preceding lake highstands from Rockwell and Sieh (1994) are shown above the new Coachella lake chronology. Dates of early expeditions to the region from Lippincott (2007) are shown by vertical dashed black lines; D/A: Díaz/Alarcón, O: Oñate, K: Kino, A: Anza.

elevation. However, this early study relied on relatively few carbon dates, most of which were shells (susceptible to the aforementioned old-carbon reservoir effect). The Coachella lake sequence, obtained using a larger date population and modern dating methods, is almost certainly more accurate.

Preliminary data from the Salt Creek site, located at −60 m elevation, support the interpretation that there have been 5–6 lake-filling events during the past 1200 yr (Williams, 2009), suggesting that periods of desiccation were usually long enough for Lake Cahuilla to shrink to the size of the Salton Sea. The complete lake chronology for the Indio site (located at the paleoshoreline) has never been published (Sieh, personal commun., 2006). However, ages of subaerial samples immediately below lacustrine transgressions from the Indio site and other shoreline sites have been published in abstract form and represent times shortly prior to lake highstand (Rockwell and Sieh, 1994). These dates (shown by an X in Fig. 18) are potentially consistent with the Coachella lake chronology, given the dating uncertainties. Incomplete and less well-dated lake chronologies have been reported from the Superstition Mountain (Gurrola and Rockwell, 1996), International Border (Thomas and Rockwell, 1996), and Brawley (Meltzner *et al.*, 2006) paleoseismic sites (see locations on Fig. 1b), at the 12-m highstand shoreline, 9 m elevation, and −37 m, respectively. While none of these chronologies has sufficient stratigraphic resolution or age control to make a useful comparison with the Coachella lake chronology, they are generally consistent with this chronology. All three studies suggest that the most recent lake highstand occurred during the late 1600s, and that the penultimate lake filled during the mid- to late-1400s. Additionally, a recent study of the deep basin stratigraphy below the Salton Sea is generally consistent with our nearshore stratigraphy, supporting the hypothesis that the basin did not desiccate completely between the most recent three highstands (Brothers, 2009).

There is no lake in Waters' (1983) sequence that corresponds with the most recent lake found at Indio and Coachella, but his sequence may be shifted backward in time due to the shell reservoir effect, and/or the thin deposits of the most recent lake may have been eroded away at his sites as they were in the eastern trench at the Coachella site. Waters (1983) argued that Lake Cahuilla could not have filled after A.D. 1540 based on expeditions made by Spanish explorers up the Colorado River to the settlement that is now Yuma, Arizona. These expeditions were led by Díaz and

Alarcón in 1540, Oñate in 1604–1605, Kino in 1700–1702, and Anza in 1774 (Lippincott, 2007; see Fig. 18). However, the expeditions prior to 1774 documented only the course of the river; travelers would not necessarily have noticed whether a lake was present in the Salton Trough if it was disconnected from the river, because the extremely flat terrain in the vicinity of the river makes it impossible to see over the horizon into the Salton Trough. Explorers of the 1605 Oñate and 1702 Kino expeditions were told by local American Indians about a lake to the north, but none went to investigate (Lippincott, 2007). Because it is estimated that the lake would require only 10–20 yr to fill completely if the entire flow of the Colorado River was diverted (Waters, 1983), the lake could easily have filled during both the 1540–1604 and 1605–1700 time intervals but then disconnected from the river before the next expedition arrived. According to the approximate lake chronology shown in Figure 18, the Oñate and Kino expeditions traveled during periods when the lake was not receiving river influx. The Díaz and Alarcón expeditions of 1540 are the most difficult to reconcile with our lake chronology, as this year falls in the middle of the estimated duration of the second youngest lake. The lake would require a substantial influx (perhaps 50% of the Colorado River flow) to sustain its 12 m elevation, but it is not impossible that the Colorado delta fed both the lake and the ocean for a period of time. If the explorers' observations truly indicate that the lake was disconnected from the river in 1540, the most likely explanation is that the second youngest lake filled after 1540, and the older detrital charcoal sample ages are too old to accurately represent the age of deposition.

Lake Triggering

Seismicity exhibits seasonal cycles in some regions, illustrating that the seemingly minor weight of accumulated rainwater or snow can trigger or inhibit fault failure (e.g., Heki, 2003; Bollinger *et al.*, 2007). The filling of large artificial reservoirs commonly triggers seismicity (Simpson *et al.*, 1988; Gupta, 2002), and the filling and emptying of pluvial Lake Bonneville has been cited as a possible cause for Holocene slip rate variations on several Great Basin normal faults (Hetzel and Hampel, 2005). The presence of soft-sediment deformation at the Coachella site indicates that the most recent earthquake occurred just after the last highstand of the lake, demonstrating correlation if not causation. In light of the assessment that there were at least five major ruptures of the southernmost SAF during the ~800 yr between A.D. 900 and 1700, the past 300 + yr of quiescence appears even more anomalous, leading to the hypothesis that the higher frequency of earthquakes in the past may have been linked to stress changes due to the repeated filling and emptying of Lake Cahuilla.

The lake is believed to have filled via the Rio Paredones–New River and Alamo River, former distributary channels of the Colorado River delta (Van de Kamp, 1973). The diversion of the river would have occurred near the apex of the delta (located near the intersection of the California, Arizona, and Mexico borders), from which point a minor alteration in course could send the meandering river into the Salton Trough (see Fig. 1b). However, once diverted into the Salton Trough, it is unlikely that the river would change course back toward the ocean until the lake was full, due to the favorable base level of the Trough in comparison to the Gulf of California (an effect demonstrated by the inadvertent filling of the Salton Sea in the early twentieth century). Thus, the filling of the lake is inferred to have always occurred quite rapidly and could have produced abrupt stress changes. After the lake filled, the level could be maintained for significant periods of time while any excess water spilled over the 12-meter-elevation sill separating the Salton Trough from the Gulf of California. During highstands, the lake would have covered much of the SAF trace from the Coachella Valley southward, at depths up to 90 m. Once the river diverted back into its normal path to the ocean and ceased to feed the lake, the lake would recede due to desiccation, becoming completely dry after ~60 yr (Waters, 1983), a more gradual stress change perhaps less likely to induce an earthquake.

For the vertical SAF, the filling of Lake Cahuilla would have three potential effects on fault stress: the weight of the water would increase the normal stress on the fault plane (inhibiting failure), the pore pressure would increase (promoting failure), and flexure of the earth's crust near the edges of the lake due to viscoelastic deformation would have produced local horizontal compression and extension (inhibiting or promoting failure depending on the location of the fault relative to the crust's inflection points). These effects would then be reversed when the lake emptied. Based on observed isostatic rebound since the desiccation of the most recent lake, Luttrell *et al.* (2007) modeled the stress changes that would have been produced by Lake Cahuilla and concluded that the maximum Coulomb stress changes could have been on the order of 1 MPa (but perhaps were much smaller). While this is an order of magnitude lower than the stress relieved by a typical earthquake, the lake cycle could conceivably have increased the Coulomb stress enough to trigger an earthquake if the SAF was already close to failure, or it could have decreased the stress enough to delay fault rupture. On the parts of the fault submerged by the lake, after a filling event the likelihood of fault rupture would have immediately increased due to pore pressure effects but then gradually decreased over many decades or even hundreds of years due to the viscoelastic effect. The emptying of the lake would have produced equal and opposite effects.

Luttrell *et al.* (2007) calculate Coulomb stress curves over time based on Waters' (1983) lake chronology, which (as discussed previously) is not consistent with modern carbon-14 dating, and compare this with the Thousand Palms earthquake chronology (Fumal, Rymer, and Seitz, 2002). Notwithstanding the possible errors in Waters' chronology, this combination of an earthquake record and a lake record from two spatially separated sites, correlated only via radiometric dating, is not a very reliable determination of the

relative timing of earthquakes and lakes. The relative timing we deduce from the stratigraphy at the Coachella site is independent of any errors in carbon dating or correlation of units between distant sites, and thus provides a better test of the lake-triggering model.

For our results, the earthquakes do not tend to occur at any particular stage in the lake cycle. Coa-1 occurred as the lake was beginning to recede from highstand, Coa-2 and Coa-6 (if the latter is a real earthquake) occurred toward the later end of lake highstands, Coa-4 occurred in the middle of a long subaerial interval, Coa-5 and Coa-7 occurred shortly prior to lake highstands, and the exact earthquake horizon of Coa-3 (if a real earthquake) is uncertain. According to the model put forth by Luttrell *et al.* (2007), the most likely time for triggered earthquakes would be shortly after a lake filled, but none of the earthquakes in the Coachella chronology definitively occurred in such a circumstance. It is possible that a more precise model of the stress history based on the Coachella lake chronology would reveal correlations with time-delayed stress changes related to the viscoelastic affect, but the Coachella record argues against immediate triggering of earthquakes by lake receding or filling.

The only potential relationship that can be observed in the earthquake-lake history is that at least four out of the seven earthquakes occurred shortly prior to a time when the lake either receded or filled. Because it would take a decade or more for the lake to fill up to the level of the Coachella site and a few years to drop from the 12-m high shoreline, it could be argued that these earthquakes were triggered by the early stages of the filling and desiccation processes. However, given that even the maximum possible stress change is small, the even lesser changes in stress that would have occurred early in the filling or emptying processes are highly unlikely to have triggered earthquakes. A more likely possibility is that, rather than the lake cycle triggering earthquakes, earthquakes have triggered shifts in the course of the Colorado River that led to the filling or emptying of Lake Cahuilla. This hypothesis also explains the similarity between the frequencies of earthquakes and lakes, and is consistent with the observation that most of the earthquakes in the Coachella record appear to have preceded a lake-filling or receding event. While the precise mechanisms by which the river was diverted are not known, the very low relief, young unconsolidated sediments, and meandering riverbed of the Colorado River delta could permit seismically induced liquefaction and lateral spreading of the river bank sufficient to divert the river.

Conclusions

The Coachella paleoseismic site study provides evidence for 5–7 earthquakes since A.D. 900. The average recurrence interval is 116–135 yr (probable and possible events) or 174–202 yr (probable events only). If the current open interval of ~320 yr is included, these estimates increase to 150–158 yr and 210–221 yr. However, no matter which of these estimates is most accurate, the current interseismic interval is significantly longer than the average and is approaching the length of the longest observed ~340-yr interval (present between Coa-2 and Coa-4, if Coa-3 did not occur). If all seven of the proposed earthquakes did occur, the current open interval is significantly longer than any of the observed intervals. There can be little doubt that major or great earthquakes rupture the southernmost SAF on average every ~200 yr; therefore the current 300-yr open interval indicates a high probability of rupture in the near future.

The Coachella site has also provided the most complete well-dated stratigraphy recording the history of ancient Lake Cahuilla. There have been 5–6 highstands of the lake since A.D. 800. The similarity of the lake frequency and the earthquake frequency, as well as the correlation in time between the most recent lake and the most recent earthquake, suggests a connection between the two. While earthquakes have not consistently occurred during any particular stage in the lake cycle, future modeling with our more accurate lake chronology may reveal that the earthquake record expresses some effects of lacustrine stress. However, given that many of the earthquakes recorded at the Coachella site appear to have shortly preceded a filling or receding of the lake, it is more likely that the earthquakes trigger changes in lake level rather than the reverse.

Data and Resources

All data used in this paper came from published sources listed in the references.

Acknowledgments

This research was funded by USGS NEHRP grant #07HQGR0019, USGS grant #06HQAG0143, and internal funding from the University of Oregon. Belle Philibosian was supported by a National Science Foundation Graduate Research Fellowship. We are extremely grateful to Rilington Communities for granting access to their property and to Matt Cohrt and Doug Cook of Sladden Engineering for accommodating our study. We would like to thank Katherine Kendrick, Kate Scharer, Sean Bemis, Reed Burgette, Beth Wisely, Nissa Morton, and Mike O'Bleness for their invaluable assistance in the field; Malcolm Britton, Lorna Crider, Tyler Claycomb, and Sarah Hunt for assistance with image processing; and Ken Hudnut of USGS for assistance with funding acquisition and LiDAR data. For assistance with carbon dating, we thank Michaele Kashgarian and Paula Zermeno of the Center for Acceleration Mass Spectrometry at Lawrence Livermore National Laboratory, Douglas Kennett and Brian Culleton of the Coastal Archaeology and Human Ecology Laboratory at the University of Oregon, and John Southon of the Keck Carbon Cycle Accelerator Mass Spectrometry Laboratory at the University of California, Irvine. This paper was greatly improved thanks to thoughtful reviews by Katherine Kendrick, Rob Langridge, Tom Rockwell, and Pat Williams.

References

Akciz, S. O., L. G. Ludwig, and J. R. Arrowsmith (2009). Revised dates of large earthquakes along the Carrizo section of the San Andreas fault, California, since A.D. 1310 ± 30, *J. Geophys. Res.* **114,** B01313, doi 10.1029/2007JB005285.

Behr, W. M., D. H. Rood, K. E. Fletcher, N. Guzman, R. Finkel, T. C. Hanks, K. W. Hudnut, K. J. Kendrick, J. P. Platt, W. D. Sharp, R. J. Weldon,

and J. D. Yule (2010). Uncertainties in slip-rate estimates for the Mission Creek strand of the southern San Andreas fault at Biskra Palms Oasis, southern California, *GSA Bull.* **122,** 1360–1377.

Bevis, M., K. Hudnut, D. Brzezinska, R. Sanchez, and C. Toth (2006). The B4 LiDAR survey of the southern San Andreas and San Jacinto faults, *Seismol. Res. Lett.* **77,** 311.

Biasi, G. P., R. J. Weldon, T. E. Fumal, and G. G. Seitz (2002). Paleoseismic event dating and the conditional probability of large earthquakes on the southern San Andreas fault, California, *Bull. Seismol. Soc. Am.* **92,** 2761–2781.

Bollinger, L., F. Perrier, J.-P. Avouac, S. Sapkota, U. Gautam, and D. R. Tiwari (2007). Seasonal modulation of seismicity in the Himalaya of Nepal, *Geophys. Res. Lett.* **34,** L08304, doi 10.1029/2006GL029192.

Bronk Ramsey, C. (2009). Bayesian analysis of radiocarbon dates, *Radiocarbon* **51,** 337–360.

Brothers, D. S. (2009). New insights into deformation along the North America-Pacific plate boundary from Lake Tahoe, Salton Sea and southern Baja California, *Ph.D. Thesis*, University of California, San Diego, San Diego, California.

Felzer, K. R., T. W. Becker, R. E. Abercrombie, G. Ekström, and J. R. Rice (2002). Triggering of the 1999 M_w 7.1 Hector Mine earthquake by aftershocks of the 1992 M_w 7.3 Landers earthquake, *J. Geophys. Res.* **107,** 2190, doi 10.1029/2001JB000911.

Fialko, Y. (2006). Interseismic strain accumulation and the earthquake potential on the southern San Andreas fault system, *Nature* **441,** 968–971.

Fumal, T. E., M. J. Rymer, and G. G. Seitz (2002). Timing of large earthquakes since A.D. 800 on the Mission Creek strand of the San Andreas fault zone at Thousand Palms Oasis, near Palm Springs, California, *Bull. Seismol. Soc. Am.* **92,** 2841–2860.

Fumal, T. E., R. J. Weldon, G. P. Biasi, T. E. Dawson, G. G. Seitz, W. T. Frost, and D. P. Schwartz (2002). Evidence for large earthquakes on the San Andreas fault at the Wrightwood, California, paleoseismic site: A.D. 500 to present, *Bull. Seismol. Soc. Am.* **92,** 2726–2760.

Goldfinger, C., K. Grijalva, R. Bürgmann, A. E. Morey, J. E. Johnson, C. H. Nelson, J. Gutiérrez-Pastor, A. Ericsson, E. Karabanov, J. D. Chaytor, J. Patton, and E. Gràcia (2008). Late Holocene rupture of the northern San Andreas fault and possible stress linkage to the Cascadia subduction zone, *Bull. Seismol. Soc. Am.* **98,** 861–889.

Gupta, H. K. (2002). A review of recent studies of triggered earthquakes by artificial water reservoirs with special emphasis on earthquakes in Koyna, India, *Earth-Science Reviews* **58,** 279–310.

Gurrola, L. D., and T. K. Rockwell (1996). Timing and slip for prehistoric earthquakes on the Superstition Mountain fault, Imperial Valley, southern California, *J. Geophys. Res.* **101,** 5977–5985.

Heki, K. (2003). Snow load and seasonal variation of earthquake occurrence in Japan, *Earth Planet. Sci. Lett.* **207,** 159–164.

Hetzel, R., and A. Hampel (2005). Slip rate variations on normal faults during glacial-interglacial changes in surface loads, *Nature* **435,** 81–84.

Kelson, K., A. Streig, R. Koehler, and K. Kang (2006). Timing of late Holocene paleoearthquakes on the northern San Andreas fault at the Fort Ross Orchard site, Sonoma County, California, *Bull. Seismol. Soc. Am.* **96,** 1012–1028.

Kilb, D. (2003). A strong correlation between induced peak dynamic Coulomb stress change from the 1992 *M* 7.3 Landers, California, earthquake and the hypocenter of the 1999 *M* 7.1 Hector Mine, California, earthquake, *J. Geophys. Res.* **108,** 2012, doi 10.1029/2001JB000678.

Langridge, R. M., R. J. Weldon II, J. C. Moya, and G. Suárez (2000). Paleoseismology of the 1912 Acambay earthquake and the Acambay–Tixmadeje fault; Trans-Mexican volcanic belt, *J. Geophys. Res.* **105,** 3019–3037.

Lippincott, C. K. (2007). Testing the application and precision of optically stimulated luminescence on dating lacustrine shorelines in the Imperial Valley, southern California, *Master's Thesis*, San Diego State University, San Diego, California.

Luttrell, K., D. T. Sandwell, B. Smith-Konter, B. Bills, and Y. Bock (2007). Modulation of the earthquake cycle at the southern San Andreas fault by lake loading, *J. Geophys. Res.* **112,** B08411, doi 10.1029/2006JB004752.

Lyons, S., and D. T. Sandwell (2003). Fault creep along the southern San Andreas from interferometric synthetic aperture radar, permanent scatterers, and stacking, *J. Geophys. Res.* **108,** 2047, doi 10.1029/2002JB001831.

McCalpin, J. P., T. K. Rockwell, and R. J. Weldon (2009). Stratigraphic indicators of paleoearthquakes, in *Paleoseismology*, J. P. McCalpin (Editor), Elsevier, London, UK, 473–479.

McGill, S., S. Dergham, K. Barton, T. Berney-Ficklin, D. Grant, C. Hartling, K. Hobart, R. Minnich, M. Rodriguez, E. Runnerstrom, J. Russell, K. Schmoker, M. Stumfall, J. Townsend, and J. Williams (2002). Paleoseismology of the San Andreas fault at Plunge Creek, near San Bernardino, southern California, *Bull. Seismol. Soc. Am.* **92,** 2803–2840.

Meltzner, A. J., T. K. Rockwell, and L. A. Owen (2006). Recent and long-term behavior of the Brawley fault zone, Imperial Valley, California: An escalation in slip rate?, *Bull. Seismol. Soc. Am.* **96,** 2304–2328.

Naylor, M. A., G. Mandl, and C. H. K. Sijpesteijn (1986). Fault geometries in basement-induced wrench faulting under different initial stress states, *J. Struct. Geol.* **8,** 737–752.

Olsen, K. B., S. M. Day, J. B. Minster, Y. Cui, A. Chourasia, M. Faerman, R. Moore, P. Maechling, and T. Jordan (2006). Strong shaking in Los Angeles expected from southern San Andreas earthquake, *Geophys. Res. Lett.* **33,** L07305, doi 10.1029/2005GL025472.

Pezzopane, S. K., and R. J. Weldon II (1993). Tectonic role of active faulting in central Oregon, *Tectonics* **12,** 1140–1169.

Philibosian, B. (2007). Paleoseismology of the Southern San Andreas Fault at Coachella, California, *Master's Thesis*, University of Oregon, Eugene, Oregon.

Philibosian, B., T. E. Fumal, R. J. Weldon, K. J. Kendrick, K. M. Scharer, S. P. Bemis, R. J. Burgette, and B. A. Wisely (2009). Photomosaics and logs of trenches on the San Andreas Fault near Coachella, California, in *U.S. Geol. Surv. Open-File Rept. 2009-1039*.

Reimer, P., M. Baillie, E. Bard, A. Bayliss, J. Beck, C. Bertrand, P. Blackwell, C. Buck, G. Burr, K. Cutler, P. Damon, R. Edwards, R. Fairbanks, M. Friedrich, T. Guilderson, A. Hogg, K. Hughen, B. Kromer, G. McCormac, S. Manning, C. B. Ramsey, R. Reimer, S. Remmele, J. Southon, M. Stuiver, S. Talamo, F. Taylor, J. v. d. Plicht, and C. Weyhenmeyer (2004). IntCal04 terrestrial radiocarbon age calibration, 0–26 cal kyr BP, *Radiocarbon* **46,** 1029–1058.

Rockwell, T. K., and K. E. Sieh (1994). Correlation of large earthquakes using regional lacustrine stratigraphy, examples from the Salton Trough, California, *Abstr. Programs Geol. Soc. Am.* **26,** 239.

Rymer, M. J., J. Boatwright, L. C. Seekins, J. D. Yule, and J. Liu (2002). Triggered surface slips in the Salton Trough associated with the 1999 Hector Mine, California, earthquake, *Bull. Seismol. Soc. Am.* **92,** 1300–1317.

Salyards, S. L., K. E. Sieh, and J. L. Kirschvink (1992). Paleomagnetic measurements of nonbrittle deformation across the San Andreas fault at Pallett Creek, *J. Geophys. Res.* **97,** 12,457–12,470.

Scharer, K., R. Weldon, T. Fumal, and G. Biasi (2007). Paleo-earthquakes on the southern San Andreas fault, Wrightwood, California, 3000 to 1500 B.C., *Bull. Seismol. Soc. Am.* **97,** 1054–1093.

Seitz, G. G., R. J. Weldon II, and G. P. Biasi (1997). The Pitman Canyon paleoseismic record: A re-evaluation of southern San Andreas fault segmentation, *J. Geodyn.* **24,** 129–138.

Sieh, K. E. (1986). Slip rate across the San Andreas fault and prehistoric earthquakes at Indio, California, *Eos Trans. AGU* **67,** 1200, Abstract T1222C-1201.

Sieh, K. E., and P. L. Williams (1990). Behavior of the southernmost San Andreas fault during the past 300 years, *J. Geophys. Res.* **95,** 6629–6645.

Sieh, K. E., M. Stuiver, and D. Brillinger (1989). A more precise chronology of earthquakes produced by the San Andreas fault in southern California, *J. Geophys. Res.* **94,** 603–623.

Simpson, D. W., W. S. Leith, and C. H. Scholz (1988). Two types of reservoir-induced seismicity, *Bull. Seismol. Soc. Am.* **78,** 2025–2040.

Sylvester, A. G. (1988). Strike-slip faults, *Geol. Soc. Am. Bull.* **100,** 1666–1703.

Thomas, A. P., and T. K. Rockwell (1996). A 300- to 550-year history of slip on the Imperial fault near the U.S.–Mexico border; Missing slip at the Imperial fault bottleneck, *J. Geophys. Res.* **101,** 5987–5997.

U.S. Geological Survey and California Geological Survey (2006). Quaternary fault and fold database for the United States, accessed April 2006, from USGS web site: http://earthquakes.usgs.gov/regional/qfaults/.

Van de Kamp, P. C. (1973). Holocene continental sedimentation in the Salton Basin, California, a reconnaissance, *Geol. Soc. Am. Bull.* **84,** 827–848.

van der Woerd, J., Y. Klinger, K. Sieh, P. Tapponnier, F. J. Ryerson, and A.-S. Meriaux (2006). Long-term slip rate of the southern San Andreas fault from 10Be-26Al surface exposure dating of an offset alluvial fan, *J. Geophys. Res.* **111,** B04407, doi 10.1029/2004JB003559.

Waters, M. R. (1983). Late Holocene lacustrine chronology and archaeology of ancient Lake Cahuilla, California, *Quaternary Research* **19,** 373–387.

Weldon, R. J., T. E. Fumal, T. J. Powers, S. K. Pezzopane, K. M. Scharer, and J. C. Hamilton (2002). Structure and earthquake offsets on the San Andreas fault at the Wrightwood, California, paleoseismic site, *Bull. Seismol. Soc. Am.* **92,** 2704–2725.

Weldon, R. J., K. M. Scharer, T. E. Fumal, and G. P. Biasi (2004). Wrightwood and the earthquake cycle: What a long recurrence record tells us about how faults work, *GSA Today* **14,** 4–10.

Weldon, R. J., T. E. Fumal, G. P. Biasi, and K. M. Scharer (2005). Past and future earthquakes on the San Andreas fault, *Science* **308,** 966–967.

Williams, P. (2009). Paleoseismic displacement history: Coachella Valley segment, San Andreas fault, presented a *2009 SCEC Annual Meeting*.

Working Group on California Earthquake Probabilities (2008). The Uniform California Earthquake Rupture Forecast, Version 2 (UCERF 2), in *U.S. Geol. Surv. Open-File Rept. 2007-1437 and California Geological Survey Special Report 203*.

Yule, D., and K. Sieh (2001). The paleoseismic record at Burro Flats: Evidence for a 300-year average recurrence for large earthquakes on the San Andreas fault in San Gorgonio Pass, southern California, *Abstr. Programs Geol. Soc. Am.* **33,** 31.

Yule, J. D., S. J. Maloney, and L. S. Cummings (2006). Using pollen to constrain the age of the youngest rupture of the San Andreas fault at San Gorgonio Pass, *Seismol. Res. Lett.* **77,** 245.

Division of Geological and Planetary Sciences
California Institute of Technology
M/C 100-23, Caltech
Pasadena, California 91125
belle@gps.caltech.edu
(B.P.)

U.S. Geological Survey
MS 377, 345 Middlefield Rd.
Menlo Park, California 94025
tfumal@usgs.gov
(T.F.)

Department of Geological Sciences
University of Oregon
Eugene, Oregon 97403
(R.W.)

Manuscript received 5 March 2010